Journal of Computational Physics 231 (2012) 5176–5194

Contents lists available at SciVerse ScienceDirect

Journal of Computational Physics

journal homepage: www.elsevier.com/locate/jcp

Reliable reduced-order models for time-dependent linearized Euler equations

Gilles Serre [a,*], Philippe Lafon [a], Xavier Gloerfelt [b], Christophe Bailly [c]

[a] LaMSID, UMR EDF-CEA-CNRS 8193, 1, Avenue du Général de Gaulle, 92141 Clamart Cedex, France
[b] Dynfluid Laboratory, Arts et Metiers ParisTech, 151, Boulevard de l'Hôpital, 75013 Paris, France
[c] Laboratoire de Mécanique des Fluides et d'Acoustique, UMR CNRS 5509, École Centrale de Lyon, 36, Avenue Guy de Collonge, 69134 Ecully Cedex, France

ARTICLE INFO

Article history:
Received 19 April 2011
Received in revised form 13 April 2012
Accepted 16 April 2012
Available online 28 April 2012

Keywords:
Reduced-order models (ROMs)
Nonsymmetric systems
Compressible flows
Proper orthogonal decomposition (POD)
Balanced-POD
Symmetrizer
Stabilizing projection

ABSTRACT

Development of optimal reduced-order models for linearized Euler equations is investigated. Recent methods based on proper orthogonal decomposition (POD), applicable for high-order systems, are presented and compared. Particular attention is paid to the link between the choice of the projection and the efficiency of the reduced model. A stabilizing projection is introduced to induce a stable reduced-order model at finite time even if the energy of the physical model is growing. The proposed method is particularly well adapted for time-dependent hyperbolic systems and intrinsically skew-symmetric models. This paper also provides a common methodology to reliably reduce very large nonsymmetric physical problems.

1. Introduction

Development of efficient reduced-order models is becoming an active research topic in computational physics and more particularly in fluid dynamics. Responses of dynamical systems presenting extremely large degrees-of-freedom (DoF) can nowadays be computed due to the recent advances in computer technology. However, the computation time required to solve such systems becomes prohibitive especially when numerous parametric analyses are required. Moreover, such computations are almost impossible to use in control or optimization procedures. These observations lead to the conclusion that reduced-order models, *i.e.* which have much fewer DoFs, are desired.

In past decades, numerous reduced-order techniques have been developed in various domains of physics. Linear reduction methods are now well-established in control theory [3] for instance. It is commonly admitted that the reduced-order solution must be written as a linear combination of global basis functions. The key challenge is then to construct the most efficient global functions in the most inexpensive way. Approaches basically differ in the way these global basis functions are built. The methodology depends on the type of precomputed responses of the full-order model (FOM): global eigenmodes, frequency responses or temporal responses. For a linearized fluid model, these responses, sometimes referred to as high-fidelity solutions, require solving either a very large nonsymmetric eigenvalue problem, or numerous nonsymmetric high-order linear systems, or large linear dynamical systems, respectively. As a consequence, the building of global basis

* Corresponding author. Address: Département AMA, Groupe T63, 1, Avenue du Général de Gaulle, 92141 Clamart Cedex, France.
E-mail addresses: gilles_serre@hotmail.fr (G. Serre), philippe.lafon@edf.fr (P. Lafon), xavier.gloerfelt@paris.ensam.fr (X. Gloerfelt), christophe.bailly@ec-lyon.fr (C. Bailly).

0021-9991/$ - see front matter © 2012 Elsevier Inc. All rights reserved.
http://dx.doi.org/10.1016/j.jcp.2012.04.019

functions can induce a large computational cost. First, the calculation of global eigenmodes (direct and adjoint) is an extremely expensive procedure. Furthermore, eigenvalue problems are often ill-posed for compressible open flows. In particular, it is known that the application of modal reduction is impractical due to density of eigenvalues [18] and has difficulty to capture the dynamics due to multiple poles [3]. However, it is still an active research topic in the hydrodynamic stability community to only determine the unstable eigenmodes. Secondly, finding a solution of a large linear fluid system is sometimes very expensive since the linearized fluid models are not symmetric and sometimes even unstable. For instance, iterative methods can be used but the convergence remains delicate [25]. It is therefore promising to employ dynamical approaches for computing the global basis functions.

A critical step in the process of unsteady reduction is to maintain the physical and numerical stability properties of the original model in the reduced-order model. The numerical stability is especially required for long-time simulations. Preservation of the physical stability is also important for reliable stability prediction. Unfortunately, there exists few methods able to preserve the stability when the high-fidelity model is unsteady and non-normal. In the context of linearized Euler equations (LEEs), most attempts to reach a reduced-order model are based on frequency-domain approaches such as Arnoldi's method [31], POD [17,21] or balanced-POD [30] methods. The frequency-domain has been driven by aeroelastic applications and also to achieve a higher level of robustness than in the time-domain. Nevertheless, development of reliable unsteady reduced-order models for LEEs remains a real challenge. Actually, with standard L^2 inner product, a reduced model might be stable for a given number of global basis functions but unstable for other choices of size [10]. In a recent paper, Barone et al. [6] have introduced a symmetry-based inner product and have demonstrated that it is possible to obtain a robust unsteady reduced-order model for LEEs. In a same way, Rowley [26] has obtained a stable unsteady reduced-order model in the context of linearized incompressible flows with the balanced-POD method. POD based approaches seem currently to be the best solution to reduce the LEEs and particularly for open flows. This article proposes a new approach to overcome these instability problems. The specific numerical reduction of time-dependent hyperbolic systems is also discussed.

This paper is organized as follows. First, principles of model reduction techniques are introduced in the control system framework. The construction of optimal global basis functions with the snapshot-POD method is described by considering an arbitrary inner product. A particular attention is then paid to the link between the choice of the projection and the stability property of the reduced-order model. The role of the adjoint dynamical system is also examined and a generalized stabilizing projection is proposed. Secondly, the linearized Euler model is reminded and afterwards the full-order model is described. Furthermore, the adjoint LEEs are derived. Finally, academic simulations are performed to appreciate and compare optimality and stability of the reduced-order models according to the different presented projections.

2. Reduced-order models (ROMs)

The mathematical concepts of model reduction are introduced in the framework of linear control theory. Consider a state-space representation of a linear system with q inputs, p outputs and n state variables. The system is written in a matrix formulation as

$$\begin{cases} \dot{\mathbf{x}}(t) = \mathbf{A}\mathbf{x}(t) + \mathbf{B}\mathbf{u}(t) \\ \mathbf{y}(t) = \mathbf{C}\mathbf{x}(t) \\ \mathbf{x}(t_0) = \mathbf{x}_0 \end{cases}, \tag{1}$$

where $\mathbf{x}(t) \in \mathbb{R}^n$ is the state vector, $\mathbf{A} \in \mathbb{R}^{n\times n}$ is a very large sparse square matrix from the spatial discretization of the physical model, $\mathbf{B} = (\mathbf{b}_1, \ldots, \mathbf{b}_q) \in \mathbb{R}^{n\times q}$ is a rectangular matrix from the spatial discretization of source terms (supposed space–time separable), $\mathbf{u}(t) \in \mathbb{R}^q$ is the input vector from temporal excitations, $\mathbf{C} = (\mathbf{c}_1, \ldots, \mathbf{c}_p)^T \in \mathbb{R}^{p\times n}$ is a rectangular matrix from the spatial discretization of observed linear laws (specific DoFs or physical quantities for example), $\mathbf{y}(t) \in \mathbb{R}^p$ is the output vector and $\mathbf{x}_0$ is the initial state condition. The dot denotes the time derivation. The goal is to derive a reduced system with r state variables

$$\begin{cases} \dot{\mathbf{x}}_r(t) = \mathbf{A}_r\mathbf{x}_r(t) + \mathbf{B}_r\mathbf{u}(t) \\ \mathbf{y}_r(t) = \mathbf{C}_r\mathbf{x}_r(t) \\ \mathbf{x}_r(t_0) = \mathbf{x}_{0r} \end{cases}, \tag{2}$$

such as $r \ll n$ with $\mathbf{x}_r(t) \in \mathbb{R}^r$ the reduced state vector, $\mathbf{A}_r \in \mathbb{R}^{r\times r}$ the reduced matrix, $\mathbf{B}_r \in \mathbb{R}^{r\times q}$ and $\mathbf{C}_r \in \mathbb{R}^{p\times r}$. In this reduction process, note that the number of inputs and outputs remains invariant. The next section describes the different steps to construct the reduced system (2).

2.1. Reduction technique

The projection method is the most popular and efficient approach to develop a reduced-order model. The projection algorithm proceeds as follows:

- compute the approximation space of the state vector $\mathbf{V}_r = (\mathbf{\Phi}_1, \ldots, \mathbf{\Phi}_r)$, $\mathbf{V}_r \in \mathbb{R}^{n\times r}$ such as $\mathbf{x} \simeq \mathbf{V}_r\mathbf{x}_r$ where the $\mathbf{\Phi}_i$ denote the direct global basis functions or direct modes;
- replace the approximation $\mathbf{V}_r\mathbf{x}_r$ in the full-order model (1) so the new system is overdetermined;
- compute the projection space $\mathbf{W}_r = (\mathbf{\Psi}_1, \ldots, \mathbf{\Psi}_r)$ where the $\mathbf{\Psi}_i$ denote the dual global basis functions or adjoint modes;
- project $\mathbf{W}_r$ on the overdetermined system;
- obtain the reduced system (2) of dimension r with $\mathbf{A}_r = \left(\mathbf{W}_r^T\mathbf{V}_r\right)^{-1}\mathbf{W}_r^T\mathbf{A}\mathbf{V}_r$, $\mathbf{B}_r = \left(\mathbf{W}_r^T\mathbf{V}_r\right)^{-1}\mathbf{W}_r^T\mathbf{B}$ $\mathbf{C}_r = \mathbf{C}\mathbf{V}_r$ where the superscript T denotes the transpose of a matrix;
- solve the reduced dynamical system by a classical time integration method with the reduced initial condition $\mathbf{x}_{0r} = \left(\mathbf{W}_r^T\mathbf{V}_r\right)^{-1}\mathbf{W}_r^T\mathbf{x}_0$;
- obtain the original state vector $\mathbf{x}(t) \simeq \mathbf{V}_r\mathbf{x}_r(t)$.

In these steps, the main challenge is the determination of both efficient $\mathbf{V}_r$ and $\mathbf{W}_r$ subspaces in the most inexpensive way. Furthermore, $\mathbf{V}_r$ and $\mathbf{W}_r$ subspaces are generally chosen to be bi-orthonormal *i.e.* $\mathbf{W}_r^T\mathbf{V}_r = \mathbf{I}_r$ with $\mathbf{I}_r$ the r-dimensional identity matrix. This is a condition to achieve a well-conditioned reduced model and also to avoid the calculation of the inverse matrix $\left(\mathbf{W}_r^T\mathbf{V}_r\right)^{-1}$. From a practical point of view, the reduced matrix $\mathbf{A}_{r+1}$ can be built from the reduced matrix $\mathbf{A}_r$ as follows

$$\mathbf{A}_{r+1} = \begin{pmatrix} \mathbf{W}_r^T \\ \mathbf{\Psi}_{r+1}^T \end{pmatrix}\mathbf{A}\begin{pmatrix} \mathbf{V}_r & \mathbf{\Phi}_{r+1} \end{pmatrix} = \begin{pmatrix} \mathbf{W}_r^T\mathbf{A}\mathbf{V}_r & \mathbf{W}_r^T\mathbf{A}\mathbf{\Phi}_{r+1} \\ \mathbf{\Psi}_{r+1}^T\mathbf{A}\mathbf{V}_r & \mathbf{\Psi}_{r+1}^T\mathbf{A}\mathbf{\Phi}_{r+1} \end{pmatrix} = \begin{pmatrix} \mathbf{A}_r & \mathbf{W}_r^T\mathbf{A}\mathbf{\Phi}_{r+1} \\ \mathbf{\Psi}_{r+1}^T\mathbf{A}\mathbf{V}_r & \mathbf{\Psi}_{r+1}^T\mathbf{A}\mathbf{\Phi}_{r+1} \end{pmatrix}. \tag{3}$$

This recurrence avoids to have to rebuild the reduced matrix when the number of modes is increased. Furthermore, reduced matrices are dense, $\mathbf{A}_r$ has r^2 nonzero coefficients. In the following, the main concepts to construct reliable optimal $\mathbf{V}_r$ and $\mathbf{W}_r$ subspaces are introduced.

2.2. Construction of optimal $\mathbf{V}_r$ and $\mathbf{W}_r$ subspaces: POD method

2.2.1. Minimization problem

First, a weighted inner product

$$\langle \mathbf{z}_1, \mathbf{z}_2 \rangle_Q = \mathbf{z}_1^T Q \mathbf{z}_2 \tag{4}$$

is defined on $\mathbb{R}^n$, with $Q \in \mathbb{R}^{n\times n}$ a symmetric and positive definite weighting matrix. Its induced norm is $\|\mathbf{z}\|_Q = (\mathbf{z}^T Q \mathbf{z})^{1/2}$. The objective is then to find a set of r optimal global basis functions $\mathbf{\Phi}_i$ solution of the continuous minimization problem

$$\min_{\mathbf{\Phi}_1,\ldots,\mathbf{\Phi}_r} \int_{t_0}^{t_f} \left\| \mathbf{f}(t) - \sum_{i=1}^{r} \langle \mathbf{f}(t), \mathbf{\Phi}_i \rangle_Q \mathbf{\Phi}_i \right\|_Q^2 dt \tag{5}$$

subject to $\langle \mathbf{\Phi}_i, \mathbf{\Phi}_j \rangle_Q = \mathbf{\Phi}_i^T Q \mathbf{\Phi}_j = \delta_{ij}$ for $1 \leqslant i, j \leqslant r$, where δ_{ij} stands for the Kronecker symbol. In the simplest case, $\mathbf{f}(t)$ is a vector of dimension n representing a particular solution of the dynamical system (1) at time t within the temporal interval $[t_0, t_f]$. A solution to this minimization problem is characterized by the first optimal necessary conditions

$$GQ\mathbf{\Phi}_i = \lambda_i \mathbf{\Phi}_i, \quad 1 \leqslant i \leqslant r \tag{6}$$

with

$$G = \int_{t_0}^{t_f} \mathbf{f}(t)\mathbf{f}(t)^T dt. \tag{7}$$

This problem corresponds to an n-dimensional eigenvalue problem. G is also called the time-limited Gramian. Gramians are $n \times n$ positive semi-definite symmetric matrices. Now, consider a numerical approximation of the introduced Gramian

$$G \approx \sum_{j=1}^{m} \omega_j \mathbf{f}_j \mathbf{f}_j^T \tag{8}$$

where $\mathbf{f}_i := \mathbf{f}(t_i) \in \mathbb{R}^n$ for $1 \leqslant i \leqslant m$ are m particular computed solutions of the high-fidelity model at the respective times $t_1, \ldots, t_m$ within the interval $[t_0, t_f]$ and ω_i are quadrature coefficients. These solutions are also called snapshots. The numerical solution of the minimization problem is then given by

$$\mathbf{X}\mathbf{X}^T Q \mathbf{\Phi}_i = \lambda_i \mathbf{\Phi}_i, \quad 1 \leqslant i \leqslant r \tag{9}$$

with $\mathbf{X} = [\sqrt{\omega_1}\mathbf{f}_1, \ldots, \sqrt{\omega_m}\mathbf{f}_m]$ the rectangular matrix of computed snapshots. The solutions $\mathbf{\Phi}_i$ of the n-dimensional eigenvalue problem (9) are called Q-POD modes.

2.2.2. Snapshot-POD

The eigenvalue problem (9) is generally far too difficult to solve in fluid dynamics since n is very large. It is more convenient to solve a m-dimensional eigenvalue problem than a n-dimensional ones because the number m of useful snapshots is

often much smaller than the number n of DoFs. This idea named *snapshot-POD* was introduced by Sirovich [28]. First, note that since Q is symmetric and positive definite, Q possesses a Cholesky factorization $Q = LL^T$. Hence, multiplying (9) by L^T, setting $\widetilde{\mathbf{\Phi}}_i = L^T\mathbf{\Phi}_i$ and $\widetilde{\mathbf{X}} = L^T\mathbf{X}$, gives the modified eigenvalue problem

$$\widetilde{\mathbf{X}}\widetilde{\mathbf{X}}^T\widetilde{\mathbf{\Phi}}_i = \lambda_i\widetilde{\mathbf{\Phi}}_i, \quad 1 \leqslant i \leqslant r. \tag{10}$$

The *snapshot-POD* is a thus powerful method to solve the original very large eigenvalue problem. Besides, the m-dimensional eigenvalue problem $\widetilde{\mathbf{X}}^T\widetilde{\mathbf{X}}\tilde{\psi}_i = \lambda_i\tilde{\psi}_i$ is solved with $\widetilde{\mathbf{X}}^T\widetilde{\mathbf{X}} = (\mathbf{X}^TL)(L^T\mathbf{X}) = \mathbf{X}^TQ\mathbf{X}$. In addition, the rectangular matrix $\widetilde{\mathbf{X}} \in \mathbb{R}^{n\times m}$ has a Singular Value Decomposition (SVD) such as:

$$\widetilde{\mathbf{X}}\tilde{\psi}_i = \sqrt{\lambda_i}\widetilde{\mathbf{\Phi}}_i, \quad \widetilde{\mathbf{X}}^T\widetilde{\mathbf{\Phi}}_i = \sqrt{\lambda_i}\tilde{\psi}_i, \quad 1 \leqslant i \leqslant r. \tag{11}$$

Hence, the modes $\widetilde{\mathbf{\Phi}}_i$ are calculated thanks to the relation

$$\widetilde{\mathbf{\Phi}}_i = \frac{1}{\sqrt{\lambda_i}}\widetilde{\mathbf{X}}\tilde{\psi}_i, \quad 1 \leqslant i \leqslant r. \tag{12}$$

Finally, the subspaces $\mathbf{V}_r$ and $\mathbf{W}_r$ are given by

$$\mathbf{V}_r = [\mathbf{\Phi}_1, \ldots, \mathbf{\Phi}_r], \quad \mathbf{W}_r = Q\mathbf{V}_r \tag{13}$$

with

$$\mathbf{\Phi}_i = L^{-T}\widetilde{\mathbf{\Phi}}_i = \frac{1}{\sqrt{\lambda_i}}L^{-T}L^T\mathbf{X}\tilde{\psi}_i = \frac{1}{\sqrt{\lambda_i}}\mathbf{X}\tilde{\psi}_i, \quad 1 \leqslant i \leqslant r. \tag{14}$$

Thus, both $\mathbf{V}_r$ and $\mathbf{W}_r$ subspaces depend on the choice of the weighted inner product to approximate the snapshots. This tractable POD procedure is commonly called Q-POD method. In the classical definition, note that the POD modes are calculated with the L^2-inner product which just corresponds to $Q = \mathbf{I}^n$ with $\mathbf{I}_n$ the n-dimensional identity matrix.

2.3. Gramians

2.3.1. Definition and motivation

POD modes depend on the computed solutions of the full model. These solutions appear first in the Gramian matrix (7). For exemple, the energy Gramian G_e, the controllability Gramian G_c, and the observability Gramian G_o are respectively defined by

$$G_e = \int_{t_0}^{t_f}\mathbf{x}(t)\mathbf{x}(t)^T dt, \quad G_c = \int_{t_0}^{t_f} e^{\mathbf{A}t}\mathbf{B}\mathbf{B}^T e^{\mathbf{A}^T t}dt, \quad G_o = \int_{t_0}^{t_f} e^{\mathbf{A}^T t}\mathbf{C}^T\mathbf{C}e^{\mathbf{A}t}dt \tag{15}$$

and the function $\mathbf{f}$ is then respectively given by

$$\mathbf{f}(t) = \mathbf{x}(t) = \left[e^{\mathbf{A}t}\mathbf{x}_0 + \int_0^t e^{\mathbf{A}(t-\tau)}\mathbf{B}\mathbf{u}(\tau)d\tau\right], \tag{16}$$

$\mathbf{f}(t) = e^{\mathbf{A}t}\mathbf{B}$ or $\mathbf{f}(t) = e^{\mathbf{A}^T t}\mathbf{C}^T$. In control theory, the controllability and observability Gramians are known to determine essential properties of linear systems with multiple inputs and multiple outputs [3]. Thus, the controllability Gramian is used to build POD modes which are the most independent of inputs $\mathbf{u}(t)$. Furthermore, with the observability concept, it can be chosen to observe some of the DoFs or some specific linear physical quantities of interest. For example, in [9], only the pressure at wall boundary conditions is observed. In a general manner, we can also define primal Gramian and dual Gramian respectively as follows

$$G_p = \int_{t_0}^{t_f} e^{\mathbf{A}t}\widetilde{\mathbf{B}}\widetilde{\mathbf{B}}^T e^{\mathbf{A}^T t}dt, \quad G_d = \int_{t_0}^{t_f} e^{\mathbf{A}^T t}\widetilde{\mathbf{C}}\widetilde{\mathbf{C}}^T e^{\mathbf{A}t}dt \tag{17}$$

with arbitrary matrices $\widetilde{\mathbf{B}}$ and $\widetilde{\mathbf{C}}$. When the matrix $\mathbf{A}$ is asymptotically stable, infinite primal Gramian G_p^∞ and infinite dual Gramian G_d^∞ can also be defined ($t_f = +\infty$).

2.3.2. Computation of primal and dual Gramians

The primal and dual time-limited Gramians are solutions of the algebraic Lyapunov equations [3]

$$\mathbf{A}G_p + G_p\mathbf{A}^T = -\mathbf{P}_p, \quad \mathbf{A}^T G_d + G_d\mathbf{A} = -\mathbf{P}_d \tag{18}$$

with

$$\mathbf{P}_p = e^{\mathbf{A}t_0}\widetilde{\mathbf{B}}\widetilde{\mathbf{B}}^T e^{\mathbf{A}^T t_0} - e^{\mathbf{A}t_f}\widetilde{\mathbf{B}}\widetilde{\mathbf{B}}^T e^{\mathbf{A}^T t_f}, \quad \mathbf{P}_d = e^{\mathbf{A}^T t_0}\widetilde{\mathbf{C}}^T\widetilde{\mathbf{C}}e^{\mathbf{A}t_0} - e^{\mathbf{A}^T t_f}\widetilde{\mathbf{C}}^T\widetilde{\mathbf{C}}e^{\mathbf{A}t_f}. \tag{19}$$

But it seems unrealistic to solve these equations directly since the system is too large and not sparse. An efficient alternative is to numerically approximate time-limited Gramians by a quadrature knowing a set of m snapshots (8). For example, the snapshots $\mathbf{f}(t_i) = e^{\mathbf{A}t_i}\widetilde{\mathbf{B}}$ are obtained by solving the dynamical system

$$\begin{cases} \dot{\mathbf{f}}(t) = \mathbf{A}\mathbf{f}(t) \\ \mathbf{f}(t_0) = \widetilde{\mathbf{B}} \end{cases} \tag{20}$$

with a time-integration method. Similarly, the approximation of dual Gramian involves adjoint snapshots since $\mathbf{f}(t_i) = e^{\mathbf{A}^T t_i}\widetilde{\mathbf{C}}^T$. In this paper, snapshots $e^{\mathbf{A}t}\widetilde{\mathbf{B}}$ and $e^{\mathbf{A}^T t}\widetilde{\mathbf{C}}$ are respectively called primal snapshots and dual snapshots. Bui-Thanh and Willcox [9] demonstrate the importance of accurate integration of the Gramians, that is the choice of the coefficients ω_i and instants t_i. The use of this approximation rather than solving Lyapunov equations explains why they are called empirical Gramians in the literature [20]. Note that the snapshot-POD method described in Section 2.2.2 is a powerful technique to compute the r largest eigenmodes $\mathbf{\Phi}_i$ of the Gramians associated with the r largest eigenvalues. For example, the modes of G_e, G_c and G_o are respectively called energetic modes, controllable modes and observable modes. In fact, the energetic modes correspond to the classical L^2-POD modes. A physical explanation of controllable and observable modes can be found in Bagheri et al. [4], for example.

2.4. Stability properties of the reduced model

In this section, the link between the choice of the matrix Q and the preservation of the stability of the reduced model is discussed.

2.4.1. Classical Galerkin projection

In this case, we have $Q = \mathbf{I}_n$ and $\mathbf{W}_r = \mathbf{V}_r$ such as $\mathbf{V}_r^T\mathbf{V}_r = \mathbf{I}_r$. It is an orthogonal projection. This inner product ensures the stability of the reduced matrix $\mathbf{A}_r$ if the full-order matrix $\mathbf{A}$ is negative definite or normal ($\mathbf{A}\mathbf{A}^T = \mathbf{A}^T\mathbf{A}$) and stable, or yet if the POD modes are built from the infinite primal Gramian G_p^∞. In particular, one can show that this projection preserves the symmetry and the definiteness of the full-order matrix. First, suppose that the full-order matrix is symmetric or skew-symmetric then the reduced matrix is also symmetric, respectively skew-symmetric

$$\mathbf{A}_r = \mathbf{V}_r^T\mathbf{A}\mathbf{V}_r = \pm\mathbf{V}_r^T\mathbf{A}^T\mathbf{V}_r = \pm\mathbf{A}_r^T. \tag{21}$$

Secondly, suppose that the full-order matrix is positive (respectively negative) definite then the reduced matrix is positive (respectively negative) definite. Indeed, consider an arbitrary nonzero real vector $\mathbf{x}$ and $\mathbf{A}$ positive definite, then

$$\mathbf{x}^T\mathbf{A}_r\mathbf{x} = \left(\mathbf{x}^T\mathbf{V}_r^T\right)\mathbf{A}(\mathbf{V}_r\mathbf{x}) > 0 \tag{22}$$

since $\mathbf{x}^T\mathbf{A}\mathbf{x} > 0$ for all nonzero $\mathbf{x}$ by definition of positive definite matrix. Note that this definition includes also nonsymmetric matrices by considering the symmetric part $\mathbf{A} + \mathbf{A}^T$ of $\mathbf{A}$ since

$$\mathbf{x}^T\mathbf{A}\mathbf{x} = \mathbf{x}^T\left(\frac{\mathbf{A}+\mathbf{A}^T}{2} + \frac{\mathbf{A}-\mathbf{A}^T}{2}\right)\mathbf{x} = \mathbf{x}^T\left(\frac{\mathbf{A}+\mathbf{A}^T}{2}\right)\mathbf{x}. \tag{23}$$

It can be shown that the reduced matrix $\mathbf{A}_r = \mathbf{V}_r^T\mathbf{A}\mathbf{V}_r$ can never be unstable for any stable normal matrix because the numerical range is then equal to the convex hull of the spectrum of $\mathbf{A}$ [3]. For instance, the problem of the preservation of the stability does not exist in the cases of stable symmetric, skew-symmetric or yet stable orthogonal matrices. We can also show that if the POD modes are calculated from G_p^∞ then the reduced matrix is stable since G_p^∞ is the solution of the Lyapunov Equation (18) with $\mathbf{P}_p = -\widetilde{\mathbf{B}}\widetilde{\mathbf{B}}^T$ (with $t_0 = 0$). Unfortunately, snapshots are sometimes computed from other Gramians which in addition can be finite. Moreover, linearized fluid models are often non-normal and definite. Theoretically, it is well-known that if $\mathbf{A}$ is non-normal, its eigenvectors are nonorthogonal and transient growth of perturbations can occur due to the linear interference of these eigenvectors [11,13]. In addition, the numerical range of the matrix $\mathbf{A}$ may extend into the right half plane $\mathbb{C}_+$. Consequently, the Galerkin projection may turn out to be unstable even if the original full-order system is stable. The construction of an adequate $Q \neq \mathbf{I}_n$ becomes therefore a real challenge. Moreover it is well known that the L^2-POD modes are not necessarily the best modes for describing the dynamics of a particular physical dataset [26]. This is the case for non-normal physical problems for which the standard POD method does generally not capture well the transient growth [19]. To overcome this difficulty, a particular attention must be paid to the adjoint physical problem as explained afterwards.

2.4.2. General Petrov–Galerkin projection

In this case, $Q \neq \mathbf{I}_n$ and $\mathbf{W}_r \neq \mathbf{V}_r$ with the condition $\mathbf{W}_r^T\mathbf{V}_r = \mathbf{I}_r$. When a classical Galerkin projection is employed, the subspace $\mathbf{V}_r$ is generally not an approximation space for the dual problem if the full system is not symmetric. A better solution then is to build the right subspace $\mathbf{V}_r$ as an approximation of the primal problem and to build the left subspace $\mathbf{W}_r$ as an approximation of the dual problem. With this oblique projection, it is not possible to determine the definiteness or the symmetry of the reduced matrix. The preservation of the stability of the reduced matrix is therefore not ensured with the classical arguments. Note that, in the static case, the stability preservation is solved with the left projection $\mathbf{W}_r = \mathbf{A}\mathbf{V}_r$ [8] that is the Galerkin projection on the normal equation. The unsteady models are more complex since the choice $Q = \mathbf{A}^T$ does not provide a well-posed weighted inner product ($\mathbf{A}$ is not positive definite symmetric). For other choices of Q, it is however possible to study the stability of the reduced model by considering the Lyapunov stability theory [3,27]. Setting a natural

Lyapunov candidate function $\mathcal{E}(\mathbf{x}_r) = \mathbf{x}_r^T\mathbf{x}_r$ for the reduced system and $\mathbf{A}_r = \mathbf{W}_r^T\mathbf{A}\mathbf{V}_r = \mathbf{V}_r^TQ\mathbf{A}\mathbf{V}_r$, the stability of the reduced system can be investigated as follows

$$\begin{aligned}\frac{d}{dt}\mathcal{E}(\mathbf{x}_r(t)) &= \dot{\mathbf{x}}_r^T\mathbf{x}_r + \mathbf{x}_r^T\dot{\mathbf{x}}_r = (\mathbf{A}_r\mathbf{x}_r)^T\mathbf{x}_r + \mathbf{x}_r^T(\mathbf{A}_r\mathbf{x}_r) = \mathbf{x}_r^T\left(\mathbf{A}_r + \mathbf{A}_r^T\right)\mathbf{x}_r = \mathbf{x}_r^T\left(\mathbf{V}_r^TQ\mathbf{A}\mathbf{V}_r + \mathbf{V}_r^T\mathbf{A}^TQ\mathbf{V}_r\right)\mathbf{x}_r \\ &= \mathbf{x}_r^T\mathbf{V}_r^T(Q\mathbf{A} + \mathbf{A}^TQ)\mathbf{V}_r\mathbf{x}_r = (\mathbf{V}_r\mathbf{x}_r)^T(Q\mathbf{A} + \mathbf{A}^TQ)(\mathbf{V}_r\mathbf{x}_r). \end{aligned} \tag{24}$$

The theorem of Lyapunov [3] ensures that the eigenvalues λ_i of the matrix $\mathbf{A} \in \mathbb{R}^{n\times n}$ satisfy $\Re e(\lambda_i) < 0$ if and only if, for any given symmetric positive definite matrix $\mathbf{P}$, there exists a unique positive definite symmetric matrix Q satisfying the Lyapunov equation:

$$Q\mathbf{A} + \mathbf{A}^TQ = -\mathbf{P}. \tag{25}$$

Then the last identity in (24) ensures that $\frac{d}{dt}\mathcal{E}(\mathbf{x}_r(t)) < 0$ and the asymptotical stability of the reduced model since $-\mathbf{P}$ is negative definite. More precisely, the reduced L^2-energy will be monotonically decreasing. In other words, the stability of the reduced model is conditioned by a good choice of the matrix Q in adequation with the algebraic Lyapunov equation. In the following, two recent methods for computing reliable Q are presented. A stabilizing numerical procedure is then introduced to overcome the limitations of both projections.

2.5. Infinite dual Gramian based inner product: $Q = G_d^\infty$

Infinite dual Gramians G_d^∞ are solutions of the Lyapunov Equation (18) with $\mathbf{P}_d = -\widetilde{\mathbf{C}}\widetilde{\mathbf{C}}^T$ ($t_0 = 0$). Consequently, G_d^∞ can be used in the weighted inner product to ensure the stability of the reduced system according to (24). Now, we deals with the particular case of observability Gramian G_o^∞. This approach is also called balanced-POD method, well-known in the control community. This method is an efficient computation of the historic balanced truncation method for high-order systems. Balanced truncation was first introduced by Moore [23] and then by Gavronski and Juang for time-limited Gramians [14]. It is a reduction method for linear and stable control systems. It is known to preserve the asymptotical stability of the reduced system. The main goal of this approach is to eliminate simultaneously the least controllable states and the least observable ones. Balanced modes are identified by the eigenvectors of the product of the infinite Gramians $G_c^\infty G_o^\infty$. As a consequence, the balanced modes are also the Q-POD modes with $Q = G_o^\infty$. In other words, the balanced-POD method is equivalent to apply snapshot-POD method with the observability Gramian G_o^∞ as inner product [26]. Recently, balanced-POD method has been described and adapted for many outputs by Rowley [26] in the time-domain and for general multiple inputs and multiple outputs systems by Willcox and Bui-Thanh in the frequency and time domain [30,9]. An other very interesting property is that this method does not depend on the choice of the inner product for defining both controllability and observability Gramians. For instance, the adjoint system can be induced with an arbitrary inner product [19]. In the present work, we apply the balanced-POD for an initial value problem. Such a problem may be seen as a single input multiple output system

$$\begin{cases} \dot{\tilde{\mathbf{x}}} = \mathbf{A}\tilde{\mathbf{x}} + \mathbf{A}\mathbf{x}_0 \\ \mathbf{y} = \tilde{\mathbf{x}} \end{cases}, \tag{26}$$

with $\mathbf{C} = \mathbf{I}_n$, $\mathbf{B} = \mathbf{A}\mathbf{x}_0$, $\mathbf{x}_0$ the initial condition and $\tilde{\mathbf{x}}$ the translation $\mathbf{x} - \mathbf{x}_0$. It follows that the entire state variable or in other words all the DoFs are observed then the output projection method developed by Rowley [26,19] is applied. Since the output is the full state and if the adjoint system is defined with respect to the standard L^2 inner product, the initial conditions of the adjoint simulations are just the L^2-POD modes. As a consequence, the approximation of the observability Gramian needs several adjoint simulations which can represent an important computation cost.

2.6. Symmetry based inner product: $Q = H$

An important class of models are the symmetrizable hyperbolic systems. An hyperbolic system

$$\partial_t\boldsymbol{\delta}\mathbf{q} + \mathbf{E}\partial_x\boldsymbol{\delta}\mathbf{q} + \mathbf{F}\partial_y\boldsymbol{\delta}\mathbf{q} + \mathbf{R}\boldsymbol{\delta}\mathbf{q} = \mathbf{0} \tag{27}$$

is said symmetrizable if there exists a symmetric positive definite matrix $\mathbf{H} = \mathbf{H}^T > 0$ such as $\mathbf{HE}$ and $\mathbf{HF}$ are symmetric, yielding the symmetrized system

$$\mathbf{H}\partial_t\boldsymbol{\delta}\mathbf{q} + \mathbf{HE}\partial_x\boldsymbol{\delta}\mathbf{q} + \mathbf{HF}\partial_y\boldsymbol{\delta}\mathbf{q} + \mathbf{HR}\boldsymbol{\delta}\mathbf{q} = \mathbf{0} \tag{28}$$

In a recent paper [6], Barone et al. demonstrate that if the $\mathbf{H}$-inner product is used to compute the POD modes then the ROM is better posed. A key property of this inner product is that a mathematical expression for the ROM energy can be derived. The matrix $Q = H$ is a discrete formulation of the continuous matrix $\mathbf{H}$ constructed in a same manner as the full-order matrix (1). H defines an energy based inner product and a Lyapunov function if the energy of the model is preserved or monotonically decreasing. Finally, if $\mathbf{C} = \mathbf{I}_n$, the symmetrizer based inner product combined with the controllability Gramian G_c could provide better numerical results than balanced-POD method (which corresponds to observability Gramian based inner product combined with G_c).

2.7. A stabilizing projection

Unfortunately, the stability of the reduced matrix is not always guaranteed with time-limited Gramians as suggested in the previous sections. For instance, this is the case with the dual Gramian based inner product since the matrix $\mathbf{P}_d$ from (19) is not guaranteed to be positive definite at finite time [15]. This is also the case when the full matrix $\mathbf{A}$ is neutrally stable or even weakly unstable. This motivates the introduction of a stabilizing method. This issue has been recently addressed [2,7,24] by deriving a convex optimization problem to enforce the stability of the primal reduced-model. In the present study, a new effective way is proposed to guarantee the stability of the reduced model without computing an artificial left projection $\mathbf{W}_r$.

2.7.1. Principles of the stabilizing method

We look for a projection able to enforce the stability of the reduced model for all time. This is not obvious since energy can grow at finite time, due to the non-normality of the full model. The main idea here is to impose the preservation of an introduced energy into the reduced model. If an energy is preserved then the reduced-order system should be stable. This point is essential for conservative dynamical systems, for instance. For that purpose, we first define the dynamical system

$$\begin{cases} \mathbf{E}\dot{\mathbf{z}} = \mathbf{E}\widetilde{\mathbf{A}}\mathbf{z} \\ \mathbf{z}(t_0) = \mathbf{z}_0 \end{cases} \tag{29}$$

with

$$\mathbf{z} = \begin{pmatrix} \mathbf{x} \\ \hat{\mathbf{y}} \end{pmatrix} \in \mathbb{R}^{2n}, \quad \mathbf{E} = \begin{pmatrix} \mathbf{0} & \mathbf{I}_n \\ \mathbf{I}_n & \mathbf{0} \end{pmatrix} \in \mathbb{R}^{2n\times 2n}, \quad \widetilde{\mathbf{A}} = \begin{pmatrix} \mathbf{A} & \mathbf{0} \\ \mathbf{0} & -\mathbf{A}^T \end{pmatrix} \in \mathbb{R}^{2n\times 2n}. \tag{30}$$

In this definition, $\mathbf{x}$ is a solution of the primal problem and $\hat{\mathbf{y}}$ is a solution of the anti-dual problem. Note that the large matrix $\mathbf{E}\widetilde{\mathbf{A}}$ is skew-symmetric. The second step is to construct an approximation subspace $\widetilde{\mathbf{V}}_r = \begin{pmatrix} \mathbf{V}_r^p \\ \mathbf{V}_r^d \end{pmatrix}$ such that

$$\widetilde{\mathbf{V}}_r^T\mathbf{E}\widetilde{\mathbf{V}}_r = \mathbf{V}_r^{pT}\mathbf{V}_r^d + \mathbf{V}_r^{dT}\mathbf{V}_r^p = \mathbf{I}_r. \tag{31}$$

The reduced model is then built as follows

$$\underbrace{\widetilde{\mathbf{V}}_r^T\mathbf{E}\widetilde{\mathbf{V}}_r}_{\mathbf{I}_r}\dot{\mathbf{z}}_r = \underbrace{\widetilde{\mathbf{V}}_r^T\mathbf{E}\widetilde{\mathbf{A}}\widetilde{\mathbf{V}}_r}_{\widetilde{\mathbf{A}}_r}\mathbf{z}_r \tag{32}$$

which gives

$$\dot{\mathbf{z}}_r = \widetilde{\mathbf{A}}_r\mathbf{z}_r \tag{33}$$

with

$$\widetilde{\mathbf{A}}_r = \mathbf{V}_r^{dT}\mathbf{A}\mathbf{V}_r^p - \mathbf{V}_r^{pT}\mathbf{A}^T\mathbf{V}_r^d. \tag{34}$$

The reduced model (33) is now defined for both primal and anti-dual problems. $\mathbf{V}_r^p$ is an approximation subspace for the direct problem and $\mathbf{V}_r^d$ is an approximation subspace for the anti-dual problem. The stability property of this reduced model is now studied. With the Eq. (21) or (34), the reduced matrix $\widetilde{\mathbf{A}}_r$ is also skew-symmetric. Consequently, the reduced initial energy is preserved since

$$\mathbf{z}_r^T\dot{\mathbf{z}}_r = \frac{1}{2}\frac{d}{dt}\left(\mathbf{z}_r^T\mathbf{z}_r\right) = \mathbf{z}_r^T\left(\widetilde{\mathbf{V}}_r^T\mathbf{E}\widetilde{\mathbf{A}}\widetilde{\mathbf{V}}_r\right)\mathbf{z}_r = 0 \tag{35}$$

which implies

$$\mathbf{z}_r^T\mathbf{z}_r = \mathbf{z}_{r_0}^T\mathbf{z}_{r_0}, \quad \mathbf{z}_{r_0} = \widetilde{\mathbf{V}}_r^T\mathbf{E}\mathbf{z}_0 \tag{36}$$

for all time. This procedure is called L^2-stabilizing method. A Q-stabilizing method is also introduced by considering the dynamical system

$$\begin{cases} \mathbf{E}_Q\dot{\mathbf{z}} = \mathbf{E}_Q\widetilde{\mathbf{A}}_Q\mathbf{z} \\ \mathbf{z}(t_0) = \mathbf{z}_0 \end{cases} \tag{37}$$

with

$$\mathbf{E}_Q = \begin{pmatrix} \mathbf{0} & Q \\ Q & \mathbf{0} \end{pmatrix} \in \mathbb{R}^{2n\times 2n}, \quad \widetilde{\mathbf{A}}_Q = \begin{pmatrix} \mathbf{A} & \mathbf{0} \\ \mathbf{0} & -Q^{-1}\mathbf{A}^TQ \end{pmatrix} \in \mathbb{R}^{2n\times 2n}, \quad Q = Q^T > 0. \tag{38}$$

The reduced matrix is then given by

$$\widetilde{\mathbf{A}}_r = \mathbf{V}_r^{d^T} Q\mathbf{A}\mathbf{V}_r^p - \mathbf{V}_r^{p^T}\mathbf{A}^T Q\mathbf{V}_r^d. \tag{39}$$

Similarly, the reduced energy is preserved since the full matrix $\mathbf{E}_Q\widetilde{\mathbf{A}}_Q$ is skew-symmetric.

2.7.2. Practical computation of the L^2-stabilizing method

The stabilizing method requires the construction of the subspace $\widetilde{\mathbf{V}}_r$. To do that, the snapshot method is adapted to be able to consider very large systems. Let $\mathbf{Z} = \begin{pmatrix}\mathbf{X}\\ \mathbf{Y}\end{pmatrix} \in \mathbb{R}^{2n\times m}$ a snapshot matrix from the dynamical system (29). First, simulate the direct dynamical problem

$$\begin{cases}\dot{\mathbf{x}}(t) = \mathbf{A}\mathbf{x}(t)\\ \mathbf{x}(t_0) = \mathbf{x}_0\end{cases} \tag{40}$$

and store m snapshots $\mathbf{x}(t_i)$ from the temporal interval $[t_0, t_f]$ in the matrix $\mathbf{X} = [\mathbf{x}_1, \ldots, \mathbf{x}_m]$. Secondly, simulate the skew-adjoint dynamical system

$$\begin{cases}\dot{\hat{\mathbf{y}}}(t) = -\mathbf{A}^T\hat{\mathbf{y}}(t)\\ \hat{\mathbf{y}}(t_0) = \hat{\mathbf{y}}_0\end{cases} \tag{41}$$

and store again exactly m snapshots $\hat{\mathbf{y}}(t_i)$ at the same time t_i in the matrix $\mathbf{Y} = [\hat{\mathbf{y}}_1, \ldots, \hat{\mathbf{y}}_m]$. After that, form the symmetric square matrix

$$\mathbf{Z}^T\mathbf{E}\mathbf{Z} = \mathbf{Y}^T\mathbf{X} + \mathbf{X}^T\mathbf{Y} \tag{42}$$

and compute r eigenmodes $\tilde{\psi}_i$ in a matrix $\mathbf{U}_r^+$ corresponding to the r largest positive eigenvalues λ_i stored in a diagonal matrix $\mathbf{D}_r^+$. Form then both $\mathbf{V}_r^p$ and $\mathbf{V}_r^d$ subspaces

$$\begin{aligned}\mathbf{V}_r^p &= \mathbf{X}\mathbf{U}_r^+\mathbf{D}_r^{+^{-1/2}}\\ \mathbf{V}_r^d &= \mathbf{Y}\mathbf{U}_r^+\mathbf{D}_r^{+^{-1/2}}.\end{aligned} \tag{43}$$

The biorthonormality property is therefore guaranteed since

$$\widetilde{\mathbf{V}}_r^T\mathbf{E}\widetilde{\mathbf{V}}_r = \mathbf{V}_r^{p^T}\mathbf{V}_r^d + \mathbf{V}_r^{d^T}\mathbf{V}_r^p = \mathbf{D}_r^{+^{-1/2}}\mathbf{U}_r^{+^T}\mathbf{X}^T\mathbf{Y}\mathbf{U}_r^+\mathbf{D}_r^{+^{-1/2}} + \mathbf{D}_r^{+^{-1/2}}\mathbf{U}_r^{+^T}\mathbf{Y}^T\mathbf{X}\mathbf{U}_r^+\mathbf{D}_r^{+^{-1/2}} = \mathbf{D}_r^{+^{-1/2}}\mathbf{U}_r^{+^T}(\mathbf{X}^T\mathbf{Y} + \mathbf{Y}^T\mathbf{X})\mathbf{U}_r^+\mathbf{D}_r^{+^{-1/2}} = \mathbf{I}_r. \tag{44}$$

This snapshot procedure now requires two high-fidelity simulations. It is essential that the anti-dual snapshots and direct snapshots are saved at the same times $t_1, \ldots, t_m$ and are built in the same order in matrices $\mathbf{X}$ and $\mathbf{Y}$. In addition, we choose $\hat{\mathbf{y}}_0 = \mathbf{x}_0$ to have $\mathbf{z}^T\mathbf{E}\mathbf{z} = 2\mathbf{x}_0^T\mathbf{x}_0 > 0$. Indeed, the method supposes that the modulus of negative eigenvalues of the matrix $\mathbf{X}^T\mathbf{Y} + \mathbf{Y}^T\mathbf{X}$ are non-physical or negligible compared to its largest positive eigenvalues since the matrix $\mathbf{E}$ is not definite positive. A necessary condition for that is to verify $\mathbf{z}^T\mathbf{E}\mathbf{z} = 2\mathbf{x}_0^T\hat{\mathbf{y}}_0 > 0$. That explains the important role of the initial condition $\hat{\mathbf{y}}_0$ for the skew-adjoint dynamical problem. A canonical choice to guarantee this positivity is $\hat{\mathbf{y}}_0 = \mathbf{x}_0$.

2.7.3. Remarks

The computation of the Q-stabilizing procedure is similar. In the particular case of skew-symmetrizable matrices, there exists a matrix Q such as $Q\mathbf{A}$ is skew-symmetric. For such matrices, the Lyapunov Equation (25) reduces to $Q\mathbf{A} + (Q\mathbf{A})^T = \mathbf{0}$ which implies the preservation of the reduced L^2-energy. The Q-stabilizing method is therefore equivalent to the Q-POD method if the same initial condition is considered for the skew-adjoint problem. Secondly, if $\mathbf{A}$ is asymptotically stable then $-\mathbf{A}^T$ is unstable. This is why the stabilizing projection should be more adapted for hyperbolic systems which are intrinsically skew-symmetric and also for weakly unstable systems. For symmetrizable hyperbolic systems, a good choice for defining the Q-stabilizing method should be

$$\mathbf{E}_H = \begin{pmatrix}\mathbf{0} & H\\ H & \mathbf{0}\end{pmatrix}, \quad \widetilde{\mathbf{A}}_H = \begin{pmatrix}\mathbf{A} & \mathbf{0}\\ \mathbf{0} & -H^{-1}\mathbf{A}^T H\end{pmatrix} \tag{45}$$

in order to yield a conservative and energy consistent reduced-order model simultaneously. Finally, the stabilizing procedure appears as an extension of the snapshot-POD method since it is able to induce a stable reduced system even if the primal full system is unstable. Remind that the POD procedure is limited to build a monotonically stable reduced matrix $\mathbf{A}_r = \mathbf{V}_r^T Q\mathbf{A}\mathbf{V}_r$ from a globally stable full matrix $\mathbf{A}$ (but not necessarily monotonically stable) since there does not exist a symmetric definite positive matrix Q such that $Q\mathbf{A}$ is stable if $\mathbf{A}$ is unstable. That is demonstrated from the Lyapunov theory.

3. High-fidelity test model

Dynamics of small perturbations in inviscid compressible flows can be described by the Linearized Euler Equations (LEEs). For instance, LEEs associated with appropriate source terms are often used as an extension to Lighthill's analogy in

computational aeroacoustics [5] and as an efficient simplified aerodynamic model for aeroelastic predictions [16]. The LEEs are succinctly presented in this section.

3.1. LEEs

The two-dimensional nonlinear Euler equations for a perfect gas are linearized around a steady mean flow $(\bar{\rho}, \bar{\mathbf{u}}, \bar{p})$ with ρ the density, $\mathbf{u} = (u, v)$ the velocity, p the pressure, and the overbar denoting the mean value. The behavior of small perturbations $(\delta\rho, \delta\mathbf{u}, \delta p)$ is governed by the LEEs, written in a quasi-conservative form, as:

$$\partial_t \boldsymbol{\delta q} + \partial_x(\mathbf{E}\boldsymbol{\delta q}) + \partial_y(\mathbf{F}\boldsymbol{\delta q}) + \mathbf{R}\boldsymbol{\delta q} = \mathbf{s}, \tag{46}$$

with:

$$\boldsymbol{\delta q} = \begin{Bmatrix} \delta\rho \\ \bar{\rho}\delta u \\ \bar{\rho}\delta v \\ \delta p \end{Bmatrix}, \quad \mathbf{E} = \begin{pmatrix} \bar{u} & 1 & 0 & 0 \\ 0 & \bar{u} & 0 & 1 \\ 0 & 0 & \bar{u} & 0 \\ 0 & \bar{c}^2 & 0 & \bar{u} \end{pmatrix}, \quad \mathbf{F} = \begin{pmatrix} \bar{v} & 0 & 1 & 0 \\ 0 & \bar{v} & 0 & 0 \\ 0 & 0 & \bar{v} & 1 \\ 0 & 0 & \bar{c}^2 & \bar{v} \end{pmatrix}, \quad \mathbf{R} = \begin{pmatrix} 0 & 0 & 0 & 0 \\ \bar{\mathbf{u}}^T\nabla\bar{u} & \partial_x\bar{u} & \partial_y\bar{u} & 0 \\ \bar{\mathbf{u}}^T\nabla\bar{v} & \partial_x\bar{v} & \partial_y\bar{v} & 0 \\ 0 & \tilde{\gamma}\bar{\mathbf{u}}^T\nabla\bar{u} & \tilde{\gamma}\bar{\mathbf{u}}^T\nabla\bar{v} & 0 \end{pmatrix}, \tag{47}$$

$\tilde{\gamma} = \gamma - 1$ ($\gamma = 1.4$ for air), $\bar{c} = \sqrt{\gamma\bar{p}/\bar{\rho}}$ is the local speed of sound, $\mathbf{s}$ the source term and $\mathbf{R}$ the so-called reaction matrix [25]. $\mathbf{R}$ depends only on the mean velocity and is identically null for uniform mean flows. LEEs do not only support acoustic modes, but also vorticity and entropy modes. In this paper, the mean flow will be first supposed uniform to introduce model reduction concepts. The treatment of nonuniform or even unstable base flows remains much more complex theoretically and numerically [1,5] due to possible growing energy at finite time. It can be shown that this potential growing is only induced by the reaction matrix at least for isothermal and incompressible base flows. An example of classical shear flow will be presented at the end. The LEEs (46) are a symmetrizable hyperbolic system of partial differential equations. The symmetrizing matrix $\mathbf{H}$ is given by

$$\mathbf{H} = \begin{pmatrix} \alpha^2\bar{c}^2 & 0 & 0 & -\alpha^2 \\ 0 & 1 & 0 & 0 \\ 0 & 0 & 1 & 0 \\ -\alpha^2 & 0 & 0 & d \end{pmatrix}, \tag{48}$$

with $d = (\alpha^2 + 1)/\bar{c}^2$ and α is an arbitrary real nonzero parameter. Since uniform mean flows support only neutral and decaying modes, the $\mathbf{H}$-inner product must preserve the stability in the reduced model. Furthermore, this inner product is physically consistent contrarily to the L^2-inner product [6] since

$$\delta\mathbf{q}^T\mathbf{H}\delta\mathbf{q} = \alpha^2\bar{c}^2\delta\rho^2 + \bar{\rho}^2(\delta u^2 + \delta v^2) + d\delta p^2 - 2\alpha^2\delta\rho\delta p \tag{49}$$

whereas

$$\delta\mathbf{q}^T\delta\mathbf{q} = \delta\rho^2 + \bar{\rho}^2(\delta u^2 + \delta v^2) + \delta p^2. \tag{50}$$

Expression (49) has a better physical interpretation since the induced norm is homogeneous to a physical energy.

3.2. Boundary conditions

The boundary conditions are very important in the computation of compressible flows since any reflected disturbance can contaminate the numerical solution. For outgoing acoustic waves, the nonreflecting boundary conditions of Tam and Dong [29] are used. In polar coordinates (r, θ) centered at the source position, we have

$$\partial_t\boldsymbol{\delta q} + V_g\left[\frac{\partial}{\partial r}\boldsymbol{\delta q} + \frac{1}{2r}\boldsymbol{\delta q}\right] = 0, \tag{51}$$

as $r \to \infty$. The group velocity of acoustic waves V_g is given by

$$V_g = \bar{\mathbf{u}}\cdot\mathbf{e}_r + \sqrt{\bar{c}^2 - (\bar{\mathbf{u}}\cdot\mathbf{e}_\theta)^2} \tag{52}$$

where $\mathbf{e}_r$ and $\mathbf{e}_\theta$ are the unit vectors in the r and θ directions. For an outflow boundary condition, the pressure disturbance is still considered as an acoustic fluctuation, which is not the case for the velocity and density disturbances. For these last two variables, LEEs are employed. The slip boundary condition on a wall with normal vector $\mathbf{n}$, namely $\boldsymbol{\delta u}^T\mathbf{n} = 0$, implies that there is no restriction on the velocity perturbation parallel to the wall. This slipping condition is directly substituted in the vectors $\mathbf{E}\boldsymbol{\delta q}$ and $\mathbf{F}\boldsymbol{\delta q}$ at the wall.

3.3. Semi-discretization and matrix formulation

LEEs (46) are solved on a Cartesian grid with high-order finite differences. The space derivatives are discretized with explicit centered eighth-order finite differences (non dissipative scheme). Spatial derivatives of radiation conditions (51) are solved for the three points surrounding the computational interior domain using fourth-order backward finite differences. The same backward scheme is adopted for points located near wall boundaries. A matrix formulation is adopted. The semi-discretized LEEs are thus assembled to form a global matrix and can be written in a compact form as:

$$\dot{\mathbf{x}}(t) = \mathbf{A}\mathbf{x}(t) + \mathbf{B}\mathbf{u}(t), \tag{53}$$

with $\mathbf{x}$ the unknown vector. The matrix $\mathbf{A}$ represents the discrete action of the spatial linear operator of the LEEs on the spatial discretization of the variable $\delta\mathbf{q}$. This linear system of ordinary differential equations has $n = 4 \times n_x \times n_y$ degrees of freedom where 4 is the number of physical variables, n_x and n_y the number of grid points in x and y directions respectively. Consequently, the full-order matrix $\mathbf{A}$ is block nonadiagonal and each of these blocks is also block nonadiagonal. The source term is assumed to write as a linear combination of terms where time and space variables are separable. The matrix $\mathbf{B}$ represents thus the spatial discretization of the space part of the source term $\mathbf{s}$. The matrix symmetrizer H is just block diagonal. Time integration of the full-order model (53) is performed by a fourth-order Runge–Kutta scheme.

3.4. Adjoint LEEs

Approximation of the observability Gramian and of the stabilizing projection involves respectively the adjoint matrix $\mathbf{A}^T$ and the anti-adjoint matrix $-\mathbf{A}^T$. However, it is important to notice that when a matrix formulation is adopted, the transpose of the matrix $\mathbf{A}^T$ is not always well-posed because of the boundary conditions. For example, this is the case for the radiation boundary conditions used in this study. This is explained by the fact that when the transpose of the matrix $\mathbf{A}^T$ is considered, the adjoint of the radiation boundary model is implicitly induced. But the adjoint of the Eq. (51) is not physical since it is not an asymptotic expression of the adjoint LEEs in the far field. It is then necessary to reconstruct completely the matrix from the adjoint (respectively anti-adjoint) operator with appropriate boundary conditions. The steady L^2-adjoint operator is identified for interior points after integration by parts of the LEEs over the computational domain Ω as

$$\int_\Omega \hat{\mathbf{q}}^T[\mathbf{E}\partial_x\mathbf{q} + \mathbf{F}\partial_y\mathbf{q} + \widetilde{\mathbf{R}}\mathbf{q}]d\mathbf{x} = -\int_\Omega \mathbf{q}^T[\partial_x(\mathbf{E}^T\hat{\mathbf{q}}) + \partial_y(\mathbf{F}^T\hat{\mathbf{q}}) - \widetilde{\mathbf{R}}^T\hat{\mathbf{q}}]d\mathbf{x} + \int_{\partial\Omega} \mathbf{q}^T(\mathbf{A}_n\hat{\mathbf{q}})ds \tag{54}$$

with $\widetilde{\mathbf{R}} = \mathbf{R} + \partial_x\mathbf{E} + \partial_y\mathbf{F}$. Far from the boundary conditions, the L^2-adjoint operator locally becomes

$$-\partial_x(\mathbf{E}^T\hat{\mathbf{q}}) - \partial_y(\mathbf{F}^T\hat{\mathbf{q}}) + \widetilde{\mathbf{R}}^T\hat{\mathbf{q}}. \tag{55}$$

The L^2-adjoint problem is similar to the direct problem. The sign of each characteristic is reversed so that information travels in the opposite direction. As a consequence, the Tam and Dong radiation condition remains identical. The formulation is only adapted by changing the sign of the steady mean flow in the group velocity. In the same way, the no-penetration condition is replaced in the new flux vectors. Because L^2-adjoint LEEs are of the same nature that primal LEEs, the same spatial discretization schemes for interior and boundary points and temporal integration are applied. The spatial discretization of the adjoint operator combined with adapted non-reflecting boundary condition yields a matrix $\mathbf{A}^+ \neq \mathbf{A}^T$. In a same way, the skew-adjoint operator is just obtained by changing the sign of the adjoint operator so information travels in the same direction that direct problem. Consequently, no changes of Tam and Dong boundary condition are required but again we have $-\mathbf{A}^+ \neq -\mathbf{A}^T$. In the best case, the matrix $\mathbf{A}^+$ will be conditionally asymptotically stable since the Tam and Dong boundary conditions depend on the source position. Note that LEEs are purely skew-symmetric with the symmetrizer when base flows are uniform. This property can be shown from the $\mathbf{H}$-skew-adjoint LEEs which are identical to the direct LEEs for uniform flows contrary to the L^2-skew-adjoint LEEs. Implicitly, the symmetry based inner product includes then dual information at least for uniform mean flows. Finally, since $-\mathbf{A}^T$ is not well-posed, the Q-stabilizing method is applied with the matrix

$$\widetilde{\mathbf{A}} = \begin{pmatrix} \mathbf{A} & \mathbf{0} \\ \mathbf{0} & -Q^{-1}\mathbf{A}^+Q \end{pmatrix}. \tag{56}$$

4. Numerical results

The reduced-order models are integrated in time using the same fourth order Runge–Kutta scheme with the same time step that is used in the high-fidelity simulation. Then for each numerical examples, the accuracy of the reduced model is measured from the L^2 relative error defined as the difference between a snapshot from the full-order model and from the reduced-order model

$$e_r = \max_i \frac{\|\mathbf{x}(t_i) - \mathbf{V}_r\mathbf{x}_r(t_i)\|_{L^2}}{\|\mathbf{x}(t_i)\|_{L^2}}. \tag{57}$$

Note that the H-stabilizing method is not displayed when base flows are uniform because the projection is then equivalent to the H-POD method.

Table 1
Relative error e_r as a function of the number modes and the choice of the projection.

Inner product	20	25	30	35	40	45
L^2	1.79	1.78	1.73	6.54×10^{-1}	3.61×10^{-1}	4.83×10^{-2}
$G_o - 1$	5.54×10^{-1}	9.96×10^{-2}	6.95×10^{-2}	1.35×10^{-2}	6.6×10^{-3}	9.24×10^{-4}
$G_o - 5$	4.34×10^{-1}	1.0×10^{-1}	5.68×10^{-2}	1.3×10^{-2}	5.9×10^{-3}	9.21×10^{-4}
H	2.3×10^{-1}	1.03×10^{-1}	5.47×10^{-2}	1.33×10^{-2}	6.7×10^{-3}	9.24×10^{-4}
L^2-stabilizing	2.14×10^{-1}	1.03×10^{-1}	5.47×10^{-2}	1.33×10^{-2}	6.7×10^{-3}	9.24×10^{-4}

4.1. Test with neutral stability: a critical case

This first case introduces the main numerical aspects for the construction of a reduced dynamical system. In this example, LEEs (46) are simplified to a one-dimensional propagation problem by setting periodic boundary conditions in the y-direction. An initial value problem is considered with an acoustic Gaussian pulse located at the center of the computational domain. When the simulation is performed, the propagative and retrograde waves interfere at varying positions which depend on the Mach number. For particular Mach number, this phenomenon is time-periodic. So the interference positions are repeated. Here, the period can be found by looking for the natural numbers n, m and k such as $n(c + c/k) = m(c - c/k)$. For example, for a given k, $m = k + 1$ and $n = k - 1$ can be chosen.

Table 2
$\max_i \mathcal{R}e(\lambda_i)$ as a function of the number modes and the choice of the projections.

Projections	20	25	30	35	40	45
L^2	8.36×10^{-1}	5.22×10^{-1}	3.7×10^{-1}	7.83×10^{-1}	4.85×10^{-1}	2.77×10^{-1}
$G_o - 1$	3.4×10^{-1}	6.11×10^{-2}	9.93×10^{-1}	1.33×10^{-1}	6.78×10^{-2}	2.99×10^{-2}
$G_o - 5$	5.54×10^{-2}	6.32×10^{-2}	1.9×10^{-1}	2.7×10^{-2}	8.5×10^{-3}	2.11×10^{-2}
H	4.83×10^{-15}	1.42×10^{-14}	7.55×10^{-15}	1.24×10^{-14}	1.78×10^{-14}	1.51×10^{-14}
L^2-stabilizing	3.37×10^{-14}	3.11×10^{-14}	4.26×10^{-14}	5.02×10^{-14}	5.59×10^{-14}	6.39×10^{-14}

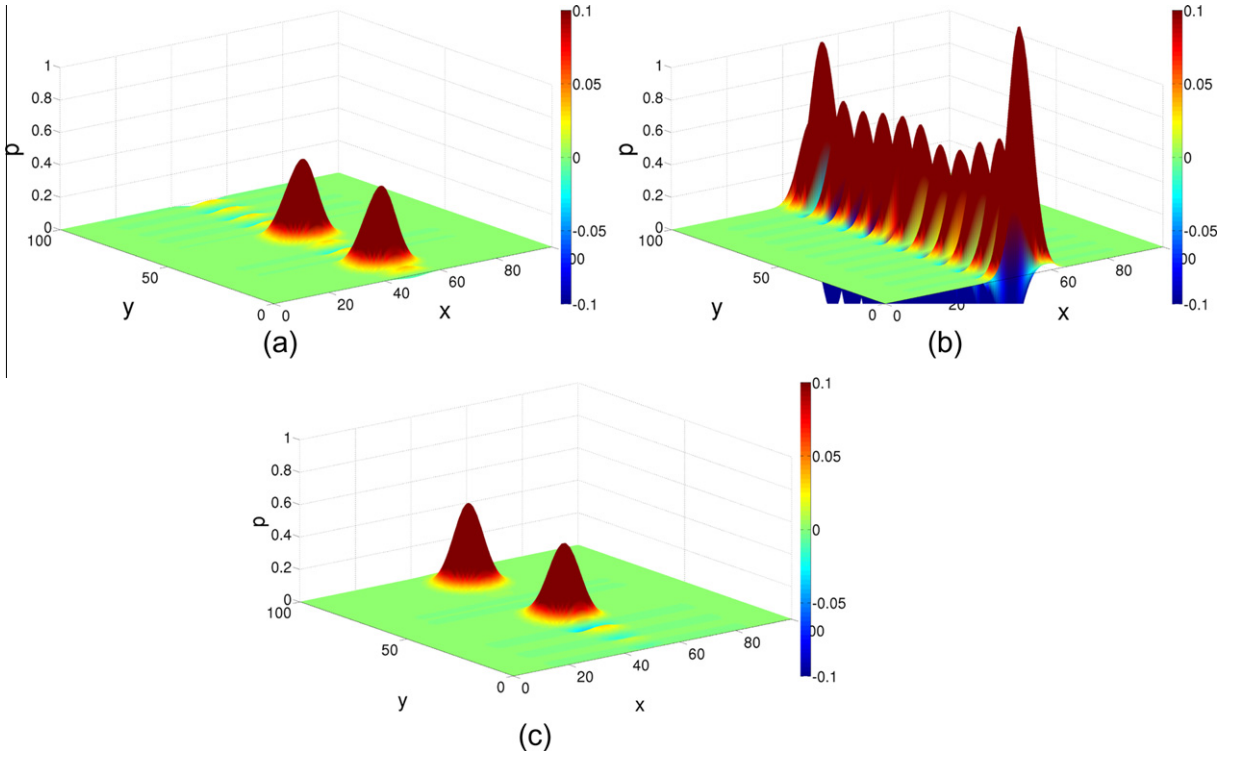

Fig. 1. Long-time behavior of reduced dynamical systems. (a) Pressure after $9000\Delta t$ with 40 L^2-POD modes, (b) Pressure after $22000\Delta t$ with 40 L^2-POD modes: development of the Galerkin instability. (c) Pressure after $350000\Delta t$ with 40 H-POD modes.

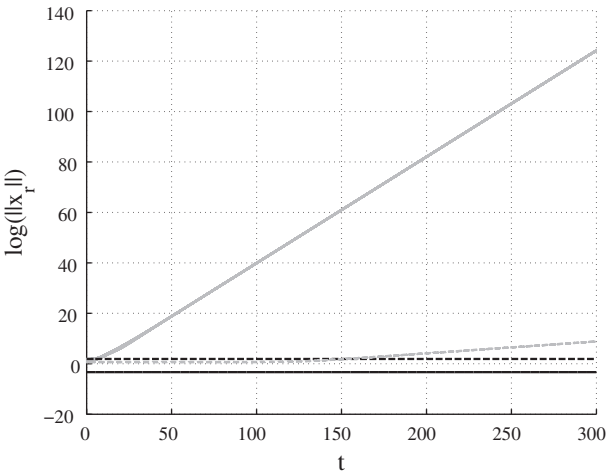

Fig. 2. Long-time behavior of the L^2-energy of the reduced dynamical systems with 50 DoFs with the different projection methods: in grey solid line: L^2, in black solid line: H, in black dashed line: L^2-stabilizing, in grey dashed line: G_o.

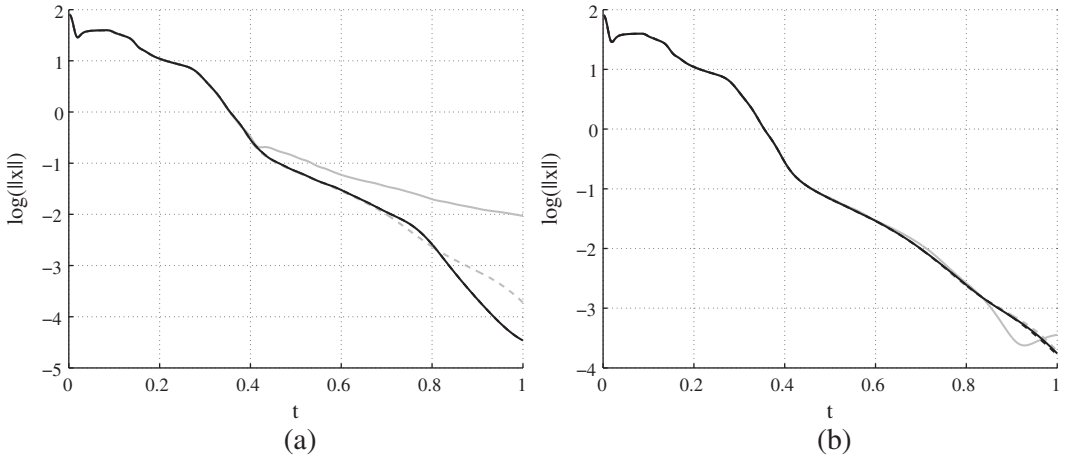

Fig. 3. Analysis of the L^2-energy decrease according to the number of modes and projections. In grey dashed line: full-order model, in grey solid line: L^2, in black solid line: H, in black dashed line: L^2-stabilizing. (a) With 30 DoFs (b) With 40 DoFs.

4.1.1. Numerical parameters

The computational domain is square with a length size of 100 m. It is discretized by 120×120 points, yielding 57600 DoFs for the full-order model. The time step is deduced from the CFL (Courant-Friedrichs-Lewy) condition. The mean flow is $(\rho_0, 0, M\bar{c}, p_0)$ with $\rho_0 = 1.2\ \mathrm{kg\,m^{-3}}$, $p_0 = 1.01325 \times 10^5$ Pa and M the Mach number. The initial condition is given by $\mathbf{q}(\mathbf{x}, t_0) = (p(\mathbf{x}, t_0)/\bar{c}^2, 0, 0, p(\mathbf{x}, t_0))^T$ with

$$p(\mathbf{x}, t_0) = \exp(-\beta[(x - x_0)^2 + (y - y_0)^2]), \tag{58}$$

$\beta = \log(2)/b^2$, $b = 5$ the half width of the Gaussian and $(x_0, y_0) = (50, 50)$ its center. Periodic boundary condition in y-direction is written for all time t as $\mathbf{q}(x, 0, t) = \mathbf{q}(x, 100, t)$.

4.1.2. Accuracy in snapshot interval

In Table 1, the accuracy of the reduced dynamical system is displayed according to the number of modes and to the projection that is used. Here the Mach number is $M = 0.5$ and consequently $k = 2$. In each case, the modes are calculated from all the snapshots in only one period which corresponds approximately 700 snapshots for $\Delta t = 0.001$ s. The G_o-POD modes are calculated from the L^2-POD modes with the output projection method proposed by Rowley and described in Section 2.5 since the state is observed everywhere in space. $G_o - 1$ and $G_o - 5$ denote respectively that the observability Gramian is calculated with one and five L^2-POD modes. H-POD modes are computed with the parameter $\alpha = 0.1$. The number of modes needed for a given accuracy depends on the half width b and as a consequence of the scale of patterns too. Both inner products H and G_o

Table 3
Relative error e_r in function of number modes and the projections.

Inner product	25	30	35	40	45	50
L^2	4.08	1.29	4.4×10^{-1}	1.11×10^{-1}	2.8×10^{-2}	5.0×10^{-3}
H	6.12×10^{-1}	1.8×10^{-1}	7.06×10^{-2}	2.15×10^{-2}	7.9×10^{-3}	3.6×10^{-3}
L^2-stabilizing	6.12×10^{-1}	1.8×10^{-1}	7.06×10^{-2}	2.15×10^{-2}	7.9×10^{-3}	3.6×10^{-3}

require fewer modes than the L^2-inner product for a given order of accuracy. Table 1 shows that the accuracy of H and G_o are very similar because they both contain dual information. This property is strengthened with the L^2-stabilizing projection that yields the same accuracy. Note also that the L^2-stabilizing projection provides exactly the same accuracy as the symmetry based inner product. Furthermore, an analogous study shows that the H, G_o and the L^2-stabilizing projection require to store less snapshots for obtaining the accuracy of the L^2-inner product.

4.1.3. Stability analysis and long-time behavior

Numerical analysis of long-time dynamics behavior of the reduced-order model can be accomplished by computing the largest real part of eigenvalues of the reduced matrix. It is indeed well-known that if this latter is lower than zero then the associated linear autonomous dynamical system is stable. In this particular numerical test, all the modes are neutral because the system is conservative. This is the reason why, the real part of all eigenvalues should be null until the machine precision. In Table 2, the largest real part of the eigenvalues of the reduced matrices induced by the different inner products are compared. It is observed that both reduced matrix constructed thanks to the L^2 and G_o inner products do not conserve the neutral

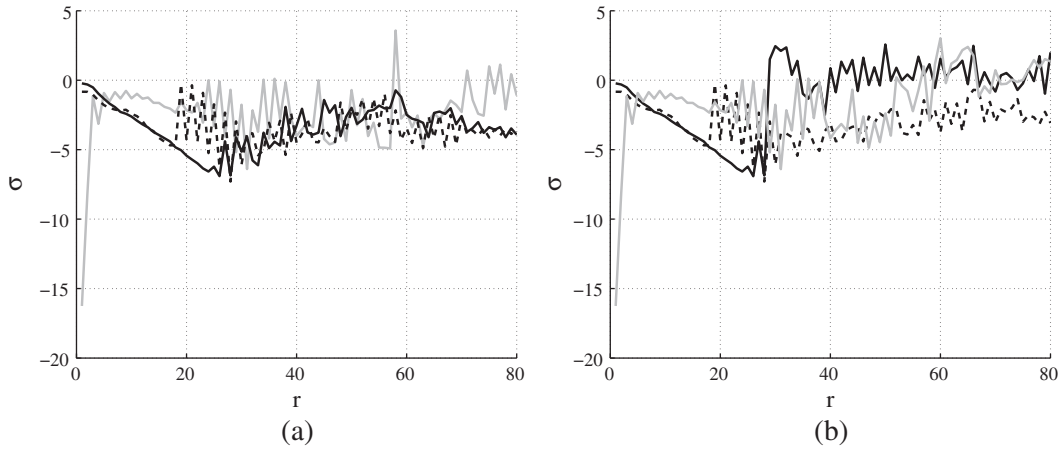

Fig. 4. Analysis of the stability of the reduced-order models according to the r number of modes, the projection and the temporal interval construction. $\sigma = \max_{1 \leqslant i \leqslant r} \mathcal{R}e(\lambda_i)$ with λ_i the eigenvalues of the reduced matrix. In grey solid line: L^2, in black solid line: H, in black dashed line: L^2-stabilizing. (a) snapshots saved in $[t_0, t_f] = [0, 0.75]$, (b) snapshots saved in $[t_0, t_f] = [0, 1]$.

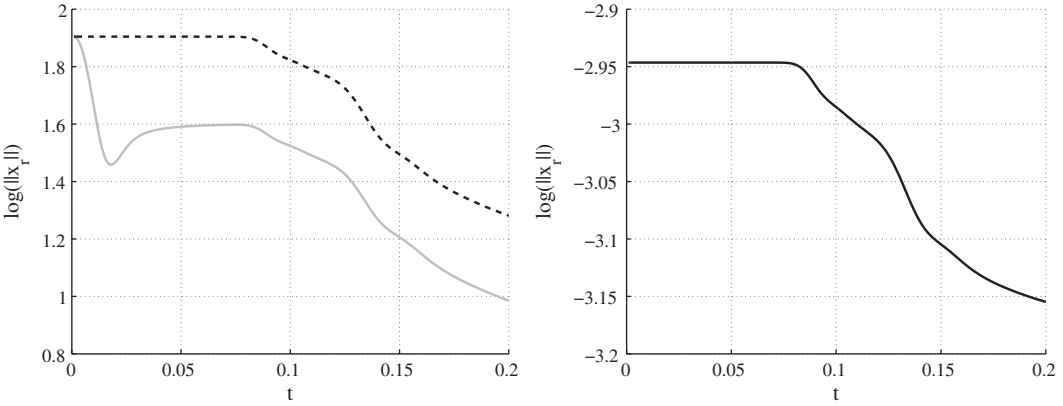

Fig. 5. Evolution of the reduced L^2-energy according to the projections. In grey solid line: L^2, in black solid line: H, in black dashed line: L^2-stabilizing.

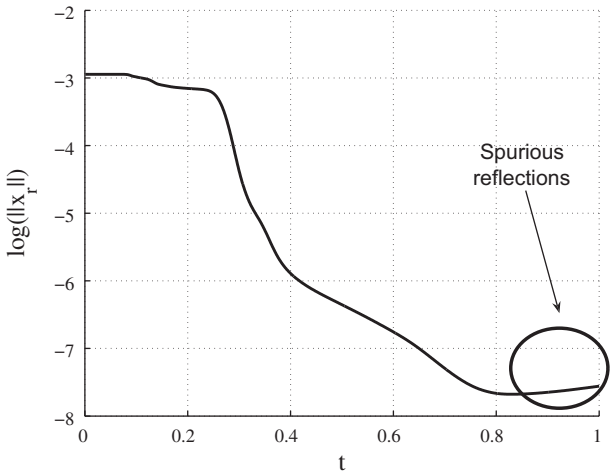

Fig. 6. Evolution of the reduced L^2-energy according to the H-projection showing growing energy at long time due to spurious reflections.

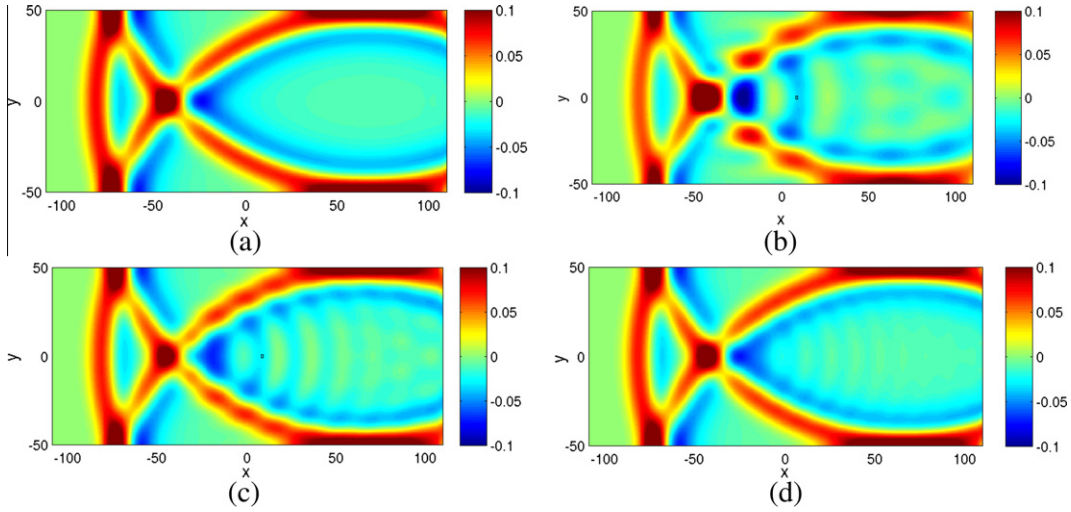

Fig. 7. Acoustic perturbation in an open channel: pressure field at $540\Delta t$. (a) Full-order model (b) ROM with 20 DoFs (c) ROM with 30 DoFs (d) ROM with 40 DoFs.

stability contrary to the H inner product. This is explained by the fact that the full model is not asymptotically stable then the infinite controllability Gramian is not defined. Note that Ma et al. [22] suggest in a recent paper to subtract the neutral modes of the full model in a first time and then to apply the balanced-POD method. This technique can not be applied to our case since all the modes are neutral. The reduced models from the symmetry projection and the stabilizing projection are perfectly neutrally stable because the reduced matrix is purely skew-symmetric. In Fig. 1, the classical Galerkin instability occurring when a L^2 projection is employed, is illustrated after some periods in pictures (a) and (b). On the contrary, the dynamical system from the H-POD modes is impressively clean after numerous periods in picture (c). In Fig. 2, the long-time behavior of the L^2-energy of the reduced model is plotted for the different projections showing that the reduced energy is not preserved with the L^2 and G_o projections in agreement with the stability analysis. On the other hand, the energy is perfectly conserved with the H and L^2-stabilizing projections.

4.2. Acoustic perturbation in an open system

In this test-case, we check if the reduced model is still numerically well-posed in the presence of radiation boundary conditions. Since the waves leave the physical domain, the full-order model should be asymptotically stable. The reduced model should then preserve this stability behavior. The observability-Gramian-based inner product is not compared here because the nonreflective boundary conditions turned out to be insufficient in simulations of the L^2-adjoint LEEs with L^2-POD modes

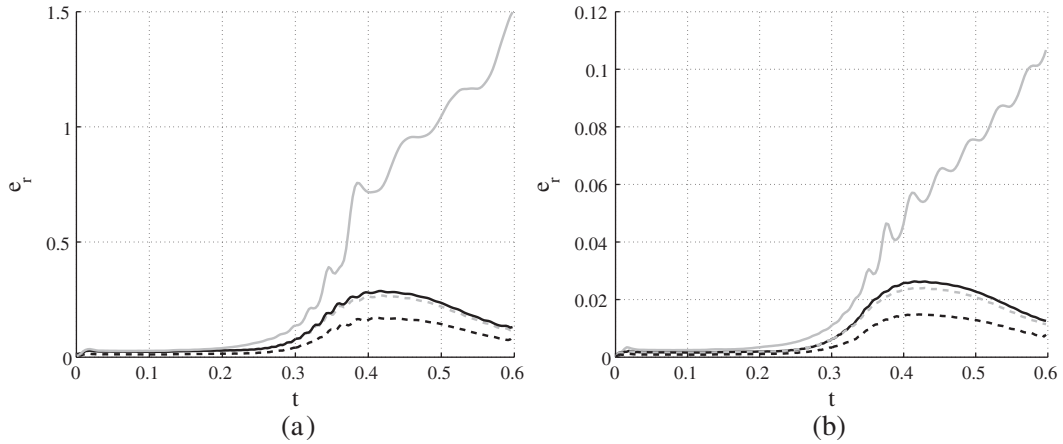

Fig. 8. Time-evolution of accuracy according to the different methods. (a) with 50 modes (b) with 70 modes. In grey solid line: L^2, in black solid line: H, in black dashed line: L^2-stabilizing and in grey dash line: H-stabilizing.

as initial conditions. Improvement of the anechoic boundary conditions for the L^2-adjoint LEEs must be carried out in future studies. The numerical parameters and the initial condition are identical to the previous test case. Non-reflecting boundary conditions are used in both spatial directions. The base flow is uniform in the x-direction with $M = 0.5$. Hence the outflow

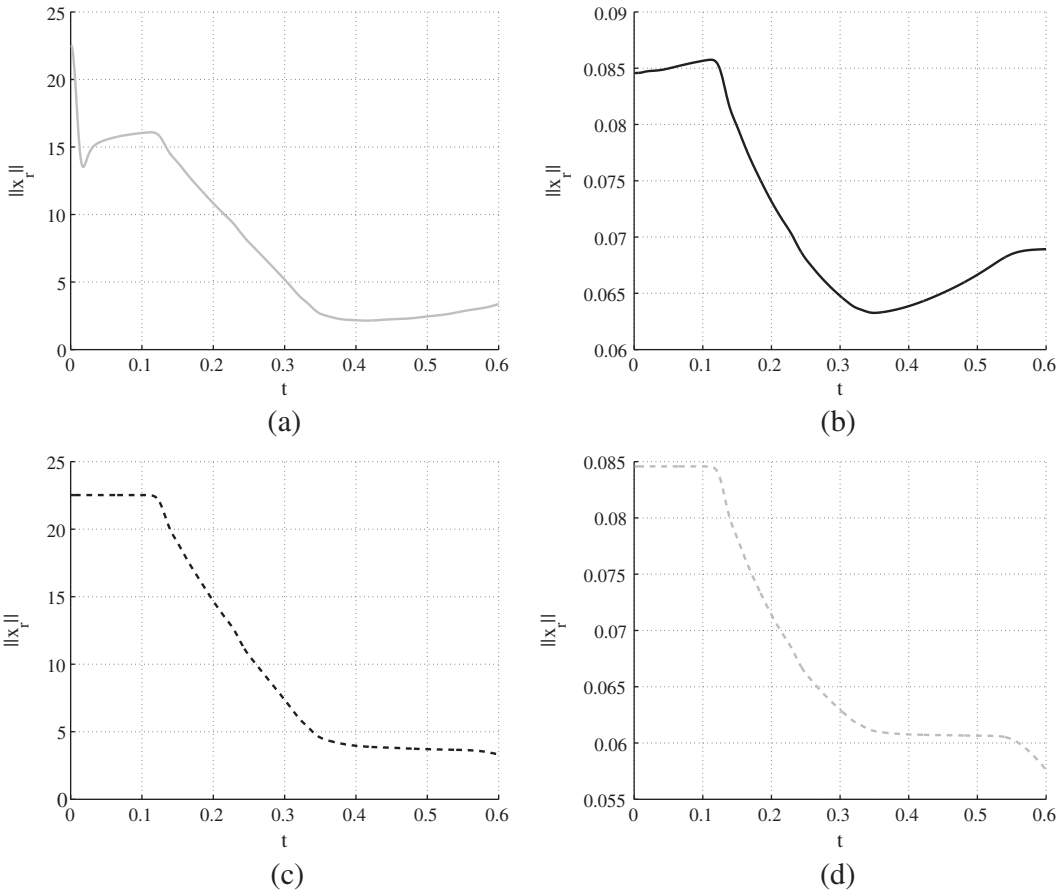

Fig. 9. L^2-Energy of the reduced model in function of the projection. (a) L^2-POD method (b) H-POD method (c) L^2-stabilizing method (d) H-stabilizing method.

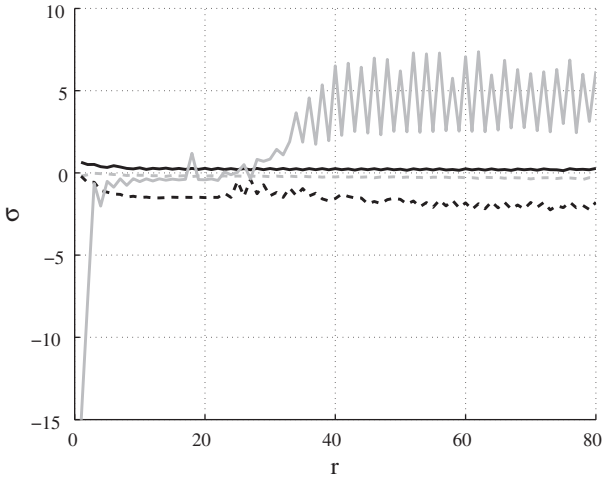

Fig. 10. Analysis of the stability of the reduced-order models according to the r number of modes and the projections. In grey solid line: L^2, in black solid line: H, in black dashed line: L^2-stabilizing, in grey dash line: H-stabilizing.

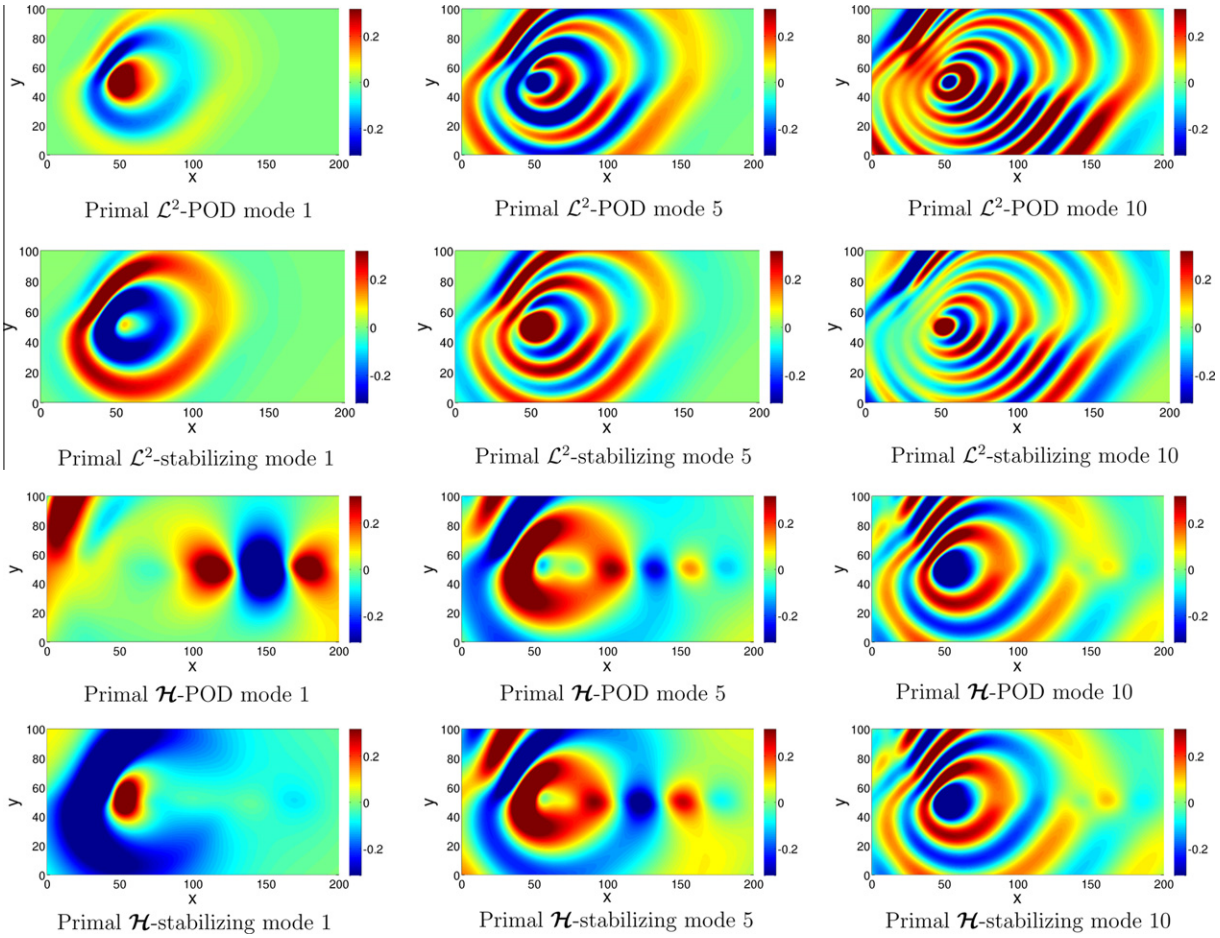

Fig. 11. Example of direct modes showing pressure field for the different methods.

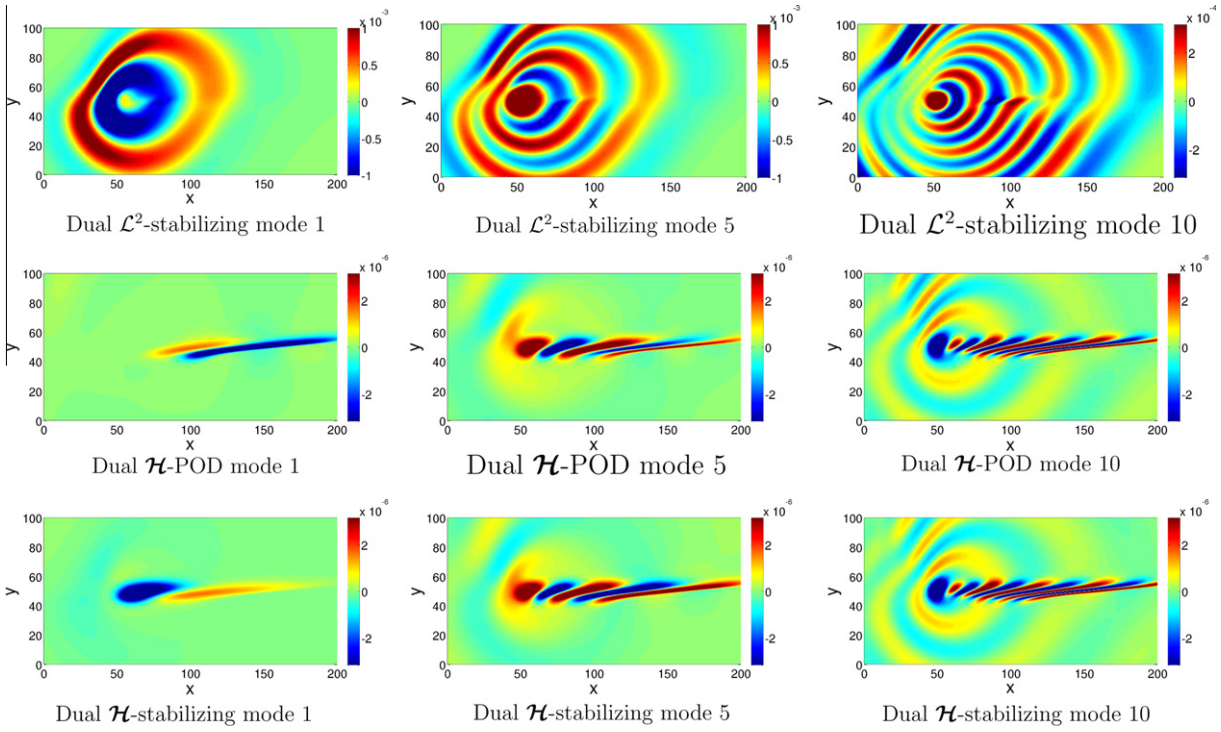

Fig. 12. Example of adjoint modes showing equivalent pressure field for the different methods.

boundary condition is placed on the right computational domain. The perturbations are recorded every two time steps. In Fig. 3, the symmetry based inner product and the L^2-stabilizing projection reproduce perfectly the dissipation of the energy in agreement to the high-fidelity simulation with forty DoFs (picture (b)). On the other hand, the L^2 projection needs more modes to reproduce faithfully the decreasing rate of the energy in the computational domain at long time. This difference is more significant with only thirty modes (picture (a)). That is also attested by the accuracy analysis given in Table 3. The stability analysis in Fig. 4(a) reveals that the L^2 projection can be unstable for certain choices of the reduced dimension contrarily to both H and stabilizing projections. In Fig. 5, it can be seen that both L^2-stabilizing method and H-POD method conserve the reduced energy as long as disturbances are far from radiation boundary conditions. In addition, energy profiles of these both methods are globally monotonic contrarily to the energy profile obtained by the standard POD method. Note that since the perturbations must leave the computational domain for the primal and the dual problem, the reduced energy can not be preserved. That also explains why the matrix $-\mathbf{A}^T$ can not be well-posed with two-dimensional non-reflecting boundary conditions. The stability analysis in Fig. 4(b) combined with the analysis of reduced energy profile in Fig. 6 shows that spurious reflections due to imperfect non-reflecting boundary conditions have consequences for the stability of the reduced matrix. Actually, the smallest non physical reflections can induce sufficient numerical growing energy to destabilize the reduced model. That also explains the difficulty for using balanced-POD method since the rigorous asymptotic behavior is then uncertain. However, the L^2-stabilizing method has been able to preserve the stability even with these spurious reflections. The development of perfectly non-reflecting boundary conditions for compressible flow remains an open topic in aeroacoustics [12].

4.3. Acoustic perturbation in an open channel

The computational domain is a 200 m $\times$ 100 m rectangle, discretized by 201 $\times$ 101 points, so that the high-fidelity model has 81204 DoFs. Radiation boundary conditions are applied in x-direction and wall boundary conditions are applied in y-direction. The same initial value problem is considered but now $(x_0, y_0) = (0, 0)$ and $\Delta t = 0.7127 \times 10^{-3}$ s. The full model is advanced in time and snapshots are stored every tenth time step. The symmetry based inner product H is employed since it has given the best results in the presence of uniform base flows. Indeed, whereas the L^2-stabilizing projection would provide similar results, it requires two high-fidelity simulations (direct and anti-adjoint). The H-POD modes are constructed with 100 snapshots from the time interval simulation. In Fig. 7, pressure snapshots after 540 temporal iterations are compared for different dimensions of the reduced-order model. In this case, the ROM needs about forty modes to reproduce faithfully the high-fidelity solution.

4.4. Free mixing layer

In this last example, the propagation of the acoustic pulse (58) in a convectively unstable shear flow

$$\bar{\mathbf{u}} = \left(0.5\bar{c} + 0.25\bar{c}\tanh\left(\frac{y-50}{5}\right), 0\right)^T \tag{59}$$

is simulated. The computational domain is a $200\,\mathrm{m} \times 100\,\mathrm{m}$ rectangle, discretized by 600×300 points, so that the high-fidelity model has 720000 DoFs. The time step is $\Delta t = 0.0006$ s. The full model is simulated during 1000 time steps and solutions are stored every fifth time step yielding 200 snapshots. First, stabilizing projections and H-POD method provide similar accuracy and behave significantly better than standard POD method, as shown in Fig. 8. Again, the L^2-POD method does not capture well the transient behavior of the energy at long time with few modes. Secondly, impressive numerical results for the stabilizing projections are reported in Figs. 9 and 10. In Fig. 10, it can be seen that both L^2-stabilizing and H-stabilizing methods yield stable reduced-order models in spite of the fact that energy is growing at long time. This property is also attested by the time history of the energy reported in Fig. 9 (c) and (d), given that time evolution of the L^2 reduced energy is globally monotonically decreasing. Again, the reduced energy is preserved as long as perturbations are far from radiation boundaries but also when only the vortical mode is convected at the end of the simulation. Furthermore, H-POD method preserves the transient physical behavior of the energy. Thus the reduced matrix cannot be stable at finite time due to energy growing. Finally, some direct and adjoint modes are respectively displayed in Figs. 11 and 12. First, L^2 and H methods generate different mode structures. Secondly, Q-stabilizing methods and Q-POD methods provide modes of similar structure. In particular, H methods capture well the structure of pressure perturbation due to the vortical mode in energetically significant modes unlike L^2 methods. Actually, it can be seen that the vorticity mode is present in L^2 methods but in the higher order modes. That confirms that the use of a weighted inner product based on the matrix H induces a better representation of the physical energy.

5. Conclusion

Optimal reduced-order models have been constructed for LEEs and applied for simple two-dimensional problems. The choice of the right and left projections has been shown to be fundamental for the optimality and the stability properties of the reduced model, particularly by including dual dynamics. When all the DoFs are observed in the presence of uniform base flows, the symmetry based inner product is shown to be the most reliable for accuracy, optimality, stability and cost considerations. This product is accurate since the adjoint system is implicitly included, stable because it is an energy-based inner product and inexpensive since it needs only one direct high-fidelity simulation. A new stabilizing projection is proposed which turns out to yield similar properties and appears to be a promising extension in the presence of non-uniform flows. The method is based on the definition of a skew-symmetric dynamical system constructed from the primal and anti-dual problems. It requires two high-fidelity simulations and emphasized the crucial role of skew-adjoint systems to build stable reduced-order models from full non-symmetric problems. In this sense, it could be used even for not symmetrizable hyperbolic systems. However, the output projection method needs several high-fidelity simulations and does not ensure the stability, in particular the conservation of the energy. The method is also not easy to carry out by including non-reflecting boundary conditions. More generally, accurate non-reflecting boundary conditions can be crucial to avoid destabilization of reduced-order models. With nonuniform mean flows, it is shown that Q-stabilizing methods are able to induce a stable reduced-order model even in the presence of an hydrodynamic instability wave. The numerical procedure is then powerful since this property is not satisfied with Q-POD methods at finite time. In addition, it seems that the stabilizing method does not affect the optimality of the reduced models. Finally, the classical L^2 Galerkin projection appears to be not adapted, leading to unstable and too sensitive reduced-order models, especially to capture transients.

References

[1] A. Agarwal, P. Morris, Calculation of sound propagation in nonuniform flows: suppression of instability waves, AIAA Journal 42 (1) (2004) 80–88.
[2] D. Amsallem, C. Farhat, Stabilization of projection-based reduced-order models, International Journal for Numerical Methods in Engineering (2012), http://dx.doi.org/10.1002/nme.4274.
[3] A. Antoulas, Approximation of large-scale dynamical systems, Advances in Design and Control (2005).
[4] S. Bagheri, L. Brandt, D.S. Henningson, Input-output analysis, model reduction and control of the flat-plate boundary layer, Journal of Fluid Mechanics 620 (2009) 263–298.
[5] C. Bailly, C. Bogey, S. Candel, Modelling of sound generation by turbulent reacting flows, International Journal of Aeroacoustics 9 (4–5) (2010) 461–489.
[6] M.F. Barone, I. Kalashnikova, D.J. Segalman, H.K. Thornquist, Stable Galerkin reduced order models for linearized compressible flow, Journal of Computational Physics 228 (2009) 1932–1946.
[7] B. Bond, L. Daniel, Guaranteed stable projection-based model reduction for indefinite and unstable linear systems, In: Proceedings of the 2008 IEEE/ACM International Conference on Computer-Aided Design, pp. 728–735, 2008.
[8] T. Bui-Thanh, Model-constrained optimization methods for reduction of parameterized large-scale systems, PhD thesis, Massachusetts Institute of Technology, 2007.
[9] T. Bui-Thanh, K. Willcox, Model reduction for large-scale CFD applications using the balanced proper orthogonal decomposition, AIAA Paper, pp. 2005–4617, 2005.
[10] T. Bui-Thanh, K. Willcox, O. Ghattas, B. van Bloemen Waanders, Goal-oriented, model-constrained optimization for reduction of large-scale systems, Journal of Computational Physics 224 (2007) 880–896.

[11] J.-M. Chomaz, Global instabilities in spatially developing flows: non-normality and nonlinearity, Annual Review of Fluid Mechanics 37 (2005) 357–392.
[12] T. Colonius, Modeling artificial boundary conditions for compressible flow, Annual Review of Fluid Mechanics 36 (2004) 315–345.
[13] B. Farrel, P.J. Ioannou, Generalized stability theory. Part I: Autonomous operators, Journal of the Atmospheric Sciences 53 (14) (1996) 2025–2040.
[14] W. Gawronski, J.-N. Juang, Model reduction in limited time and frequency intervals, International Journal of Systems Science 21 (1990) 349–379.
[15] S. Gugercin, A. Antoulas, A survey of model reduction by balanced truncation and some new results, International Journal of Control 77 (8) (2004) 748–766.
[16] K.C. Hall, A linearized Euler analysis of unsteady flows in turbomachinery. PhD thesis, Massachusetts Institute of Technology, 1987.
[17] K.C. Hall, J.P. Thomas, E.H. Dowell, Proper orthogonal decomposition technique for transonic unsteady aerodynamic flows, AIAA Journal 38 (10) (2000) 1853–1862.
[18] C.W. Hindman, Control of aeroelastic structures based on a computational reduced order modeling method, PhD thesis, University of Colorado, 2003.
[19] M. Ilak, C. Rowley, Modeling of transitional channel flow using balanced proper orthogonal decomposition, Physics of Fluids (034103) (2008).
[20] S. Lall, J. Marsden, S. Glavaski, Empirical model reduction of controlled nonlinear systems, Technical Report CIT-CDS-98-008, California Institute of Technology, 1998.
[21] T. Lieu, Adaptation of reduced order models for applications in aeroelasticity, PhD thesis, University of Colorado, 2004.
[22] Z. Ma, C. Rowley, G. Tadmor, Snapshot-based balanced truncation for linear time-periodic systems, IEEE Transactions on Automatic Control 55 (2) (2010) 469–473.
[23] B. Moore, Principal component analysis in linear systems: controllability, observability, and model reduction, IEEE Transactions on Automatic Control 26 (1) (1981) 17–32.
[24] S. Prajna, POD model reduction with stability guarantee, In: Proceedings of 42nd IEEE Conference on Decision and Control, pp. 5254–5258, 2003.
[25] P.P. Rao, P.J. Morris, Use of finite element methods in frequency domain aeroacoustics, AIAA Journal 44 (7) (2006) 1643–1652.
[26] C. Rowley, Model reduction for fluids, using balanced proper orthogonal decomposition, International Journal of Bifurcation and Chaos 15 (3) (2005) 997–1013.
[27] C. Rowley, T. Colonius, R.M. Murray, Model reduction for compressible flows using POD and Galerkin projection, Physica D 189 (2004) 115–129.
[28] L. Sirovich, Turbulence and the dynamics of coherent structures. Parts I–III, Quarterly of Applied Mathematics XLV (3) (1987) 561–590.
[29] C. Tam, Z. Dong, Radiation and outflow boundary conditions for direct computation of acoustic and flow disturbances in a nonuniform mean flow, Journal of Computational Acoustics 4 (2) (1996) 175–201.
[30] K. Willcox, J. Pereire, Balanced model reduction via the proper orthogonal decomposition, AIAA Journal 40 (11) (2002) 2323–2330.
[31] K. Willcox, J. Pereire, J. White, An Arnoldi approach for generation of reduced-order models for turbomachinery, Computers and Fluids 31 (2002) 369–389.